Syntheses and Structures of Alkyl and Aryl Halide Complexes of the Type $[(PiPr_3)_2PtH(\eta^1\text{-XR})]BAr_f$ and Analogues with Et_2O, THF, and H_2 Ligands. Halide-to-Metal π Bonding in Halocarbon Complexes

Matthew D. Butts, Brian L. Scott, and Gregory J. Kubas*

Contribution from the Chemical Science and Technology Division, MS C346, Los Alamos National Laboratory, Los Alamos, New Mexico 87545

Received May 31, 1996[⊗]

Abstract: The reaction of $Pt(PiPr_3)_3$ with SO_2 led to the formation of $(PiPr_3)_2Pt(SO_2)$ (**1**), isolated in 93% yield. The addition of $[H(OEt_2)_2]^+BAr_f$ ($BAr_f = B(3,5\text{-}(CF_3)_2C_6H_3)_4$) to **1** in ether at −78 °C afforded the solvent complex *trans*-$[(PiPr_3)_2Pt(H)(OEt_2)]BAr_f$ (**2**) in 85% isolated yield. Complex **2** served as a precursor to monodentate halocarbon complexes of the type $Pt(\eta^1\text{-XR})$. The dichloromethane complex *trans*-$[(PiPr_3)_2Pt(H)(\eta^1\text{-}ClCH_2Cl)]BAr_f$ (**3**) was isolated in 80% yield by the recrystallization of **2** from CH_2Cl_2/hexane. IR spectroscopy suggested the existence of dichloromethane binding which was confirmed by X-ray crystallography. The reaction of **2** or **3** with iodo- or bromobenzene led to the isolation of the haloarene complexes *trans*-$[(PiPr_3)_2Pt(H)(\eta^1\text{-XPh})]BAr_f$, where X = I (**4**, 87% yield) or Br (**5**, 60% yield). Both compounds were characterized spectroscopically and by X-ray crystallography. An unexpected steric interaction in **4**, suggested by molecular mechanics calculations to be significant, was rationalized in terms of halide-to-metal π bonding. The PhI complex **4** decomposed under harsh conditions to the bridging iodide compound $\{trans\text{-}[(PiPr_3)_2Pt(H)]_2(\mu\text{-I})\}BAr_f$ (**6**) which was structurally characterized. The THF adduct $[(PiPr_3)_2Pt(H)(THF)]BAr_f$ (**7**), isolated in 78% yield and also characterized by X-ray crystallography, was formed when any of the compounds **2**, **3**, **4**, or **5** was dissolved in THF. The CH_2Cl_2 complex **3** reacted with H_2 to form the dihydrogen complex *trans*-$[(PiPr_3)_2Pt(H)(\eta^2\text{-}H_2)]BAr_f$ which was characterized by NMR spectroscopy.

Introduction

Alkyl and aryl halides are among the least basic of functionalized hydrocarbon compounds.[1] Despite the fact that they are poor nucleophiles, alkyl and aryl halides have been shown to coordinate to transition metal centers to form $L_nM(\eta^1\text{-XR})$ complexes.[2] The binding of halocarbons to metal centers was first suggested by Beck and Schloter in 1978.[3] These workers proposed the existence of the dichloromethane complexes $[CpM(CO)_3(CH_2Cl_2)]PF_6$ (M = Mo, W) on the basis of infrared spectroscopy. The first crystal structure that showed unambiguously that halocarbons can act as ligands was performed on the chelating diiodo species $[Ir(PPh_3)_2(H)_2(o\text{-}C_6H_4I_2)]PF_6$ by Crabtree and co-workers.[4] The first structurally characterized monodentate halocarbon compound was the analogous MeI complex $[Ir(PPh_3)_2(H)_2(IMe)_2]PF_6$.[5]

The relatively small class of $M(\eta^1\text{-XR})$ compounds is of interest for a number of reasons. Halocarbon ligands tend to be labile, and the potential exists for equilibrium between the $L_nM(\eta^1\text{-XR})$ species and the coordinatively unsaturated Lewis acidic metal centers which can coordinate and activate Lewis bases. Coordinated alkyl halides have also been shown to be activated toward nucleophilic attack at the α-carbon.[2] Furthermore, η^1-XR species may be a representation of the arrested oxidative addition of halocarbons to metal centers by an electron transfer mechanism.[6]

While a relatively small number of complexes of bidentate or chelating iodides,[4,7] bromides,[8] chlorides,[9−12] and even fluorides[13] have been reported, all isolable *monodentate* halocarbon complexes have been those of iodides[5,14] with only two exceptions.[15,16] This paper describes in part the synthesis of complexes of the type $[(PiPr_3)_2Pt(H)(\eta^1\text{-XR})]BAr_f$, where X = Cl, Br, and I, that are the first examples of monodentate halocarbon complexes of a d^{10} metal. The structures of the aryl

[⊗] Abstract published in *Advance ACS Abstracts,* November 1, 1996.

(1) (a) McMahon, T. B.; Heinis, T.; Nicol, G.; Hovey, J. K.; Kebarle, P. *J. Am. Chem. Soc.* **1988**, *110*, 7591. (b) Lias, S. G.; Liebman, J. F.; Levin, R. D. *J. Phys. Chem. Ref. Data* **1984**, *13*, 695. (c) Staley, R. H.; Beauchamp, J. C. *J. Am. Chem. Soc.* **1975**, *97*, 5920.

(2) Kulawiec, R. J.; Crabtree, R. H. *Coord. Chem. Rev.* **1990**, *99*, 89.

(3) Beck, W.; Schloter, K. *Z. Naturforsch.* **1978**, *33B*, 1214.

(4) Crabtree, R. H.; Faller, J. W.; Mellea, M. F.; Quirk, J. M. *Organometallics* **1982**, *1*, 1361.

(5) Burk, M. J.; Segmuller, B.; Crabtree, R. H. *Organometallics* **1987**, *6*, 2241.

(6) (a) Amatore, C.; Pflüger, F. *Organometallics* **1990**, *9*, 2276. (b) Stille, J. K.; Lau, K. S. Y. *Acc. Chem. Res.* **1977**, *10*, 434.

(7) Casas, J. M.; Falvello, L. R.; Forniés, J.; Martín, A. *Inorg. Chem.* **1996**, *35*, 56.

(8) (a) Burk, M. J.; Crabtree, R. H.; Holt, E. M. *Organometallics* **1984**, *3*, 638. (b) Barceló, F.; Luhuerta, P.; Ubeda, M. A.; Foces-Foces, C.; Cano, F. H.; Martinez-Ripoll, M. *J. Chem. Soc., Chem. Commun.* **1985**, 43. (c) Solans, X.; Font-Altaba, M.; Aguiló, M.; Miravitlles, C. *Acta Crystallogr.* **1985**, *C41*, 841. (d) Cotton, F. A.; Lahuerta, P.; Sanau, M.; Schwotzer, W.; Solana, I. *Inorg. Chem.* **1986**, *25*, 3526.

(9) (a) Forniés, J.; Menjón, B.; Sanz-Carrillo, R. M.; Tomás, M.; Connelly, N. G.; Crossley, J. G.; Orpen, A. G. *J. Am. Chem. Soc.* **1995**, *117*, 4295. (b) Harrison R.; Arif, A. M.; Wulfsberg, G.; Lang, R.; Ju, T.; Kiss, G.; Hoff, C. D.; Richmond, T. G. *J. Chem. Soc., Chem. Commun.* **1992**, 1374. (c) Gomes-Carneiro, T. M.; Jackson, R. D.; Downing J. H.; Orpen A. G.; Pringle, P. G. *J. Chem. Soc., Chem. Commun.* **1991**, 317.

(10) (a) Colsman, M. R.; Newbound, T. D.; Marshall, W.; Noirot, M D.; Miller, M. M.; Wulfsberg, G. P.; Frye, J. S.; Anderson, O. P.; Strauss, S. H. *J. Am. Chem. Soc.* **1990**, *112*, 2349. (b) Newbound, T. D.; Colsman, M. R.; Miller, M. M.; Wulfsberg, G. P.; Anderson, O. P.; Strauss, S. H. *J. Am. Chem. Soc.* **1989**, *111*, 3762.

(11) Van Seggen, D. M.; Hurlburt, P. K.; Anderson, O. P.; Strauss, S. H. *J. Am. Chem. Soc.* **1992**, *114*, 10995.

(12) Bown, M.; Waters, J. M. *J. Am. Chem. Soc.* **1990**, *112*, 2442.

(13) (a) Ruwwe, J.; Erker, G.; Fröhlich, R. *Angew. Chem., Int. Ed. Engl.* **1996**, *35*, 80. (b) Kulawiec R. J.; Holt, E. M.; Lavin, M.; Crabtree, R. H. *Inorg. Chem.* **1987**, *26*, 2559. (c) Catala, R. M.; Cruz-Garritz, D.; Hills, A.; Hughes, D. L.; Richards, R. L.; Sosa, P.; Torrens, H. *J. Chem. Soc., Chem. Commun.* **1987**, 261.

S0002-7863(96)01836-7 CCC: $12.00

halide compounds offer new insights into the binding of organic halides to metal centers concerning halide-to-metal π bonding. The cationic platinum center also binds other weak donors such as THF and H_2, and generally the complexes are highly labile yet *air-stable*; i.e. N_2 and O_2 do not react, even in solution, and H_2O binds only weakly and reversibly. Such stability is very rare among complexes that bind extremely weak ligands such as dichloromethane, which coordinates here to $[(PiPr_3)_2PtH]^+$ via one rather than both of its chlorine atoms.

Results

Synthesis of a Cationic Platinum Solvent-Bound Species. The reaction of $Pt(PiPr_3)_3$ with a small excess of SO_2 (3 equiv) in ether led to the loss of one equivalent of $PiPr_3$ and the isolation of $(PiPr_3)_2Pt(SO_2)$ (**1**) in 93% yield as emerald green crystals (eq 1). Infrared spectroscopy has been shown to be a

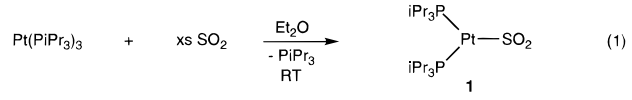

useful diagnostic tool for determining the geometry of SO_2 ligands.[17] The S−O stretching frequencies in the IR (KBr) spectrum of **1** were found at 1176 and 1035 cm^{-1} and indicate that the SO_2 is sulfur-bound in an η^1-pyramidal fashion. The same bonding mode was established some time ago for the related complex $(PCy_3)_2Pt(SO_2)$ on the basis of IR spectroscopy and X-ray crystallography.[17b] While the 3-coordinate $Pt(PiPr_3)_3$ was extremely labile in solution, there was no evidence for either SO_2 or phosphine loss from the 3-coordinate **1** in solution by $^{31}P\{^1H\}$ or ^1H NMR spectroscopy. No decomposition could be detected by NMR when solid **1** was subjected to a vacuum for several hours, indicating that the SO_2 ligand is tightly bound in the solid state as well.

The addition of $[H(OEt_2)_2]^+BAr_f$ ($BAr_f = B(3,5\text{-}(CF_3)_2C_6H_3)_4$), referred to hereafter as $HBAr_f$, to **1** at −78 °C in ether, followed by addition of hexane to precipitate the product, led to the isolation of the air stable yellow cationic ether complex $[(PiPr_3)_2Pt(H)(OEt_2)]BAr_f$ (**2**) in 85% yield (eq 2). The $^{31}P\{^1H\}$ NMR

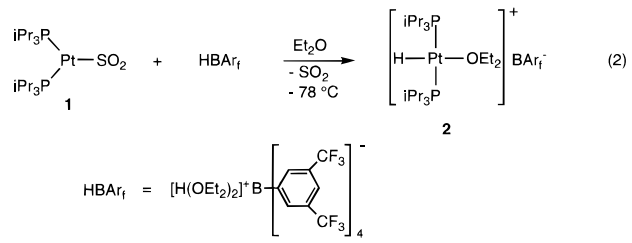

spectrum of **2** in CD_2Cl_2 at −60 °C contained only a singlet at δ 55.48, indicating that the phosphine ligands are mutually trans. The hydride resonance appeared as a triplet in the ^1H NMR spectrum (CD_2Cl_2, −83 °C) at δ −27.84 with cis coupling to the two equivalent phosphines (J_{HP} = 14 Hz). Resonances at δ 3.74 (br q) and 1.30 (t) were attributed to the CH_2 and CH_3 groups, respectively, of bound Et_2O. These were shifted downfield with respect to free ether in CD_2Cl_2 at −83 °C (δ 3.34, q; 1.08, t; both with J = 6.8 Hz as in **2**). Similarly, at −83 °C the resonances for bound ether were found in the $^{13}C\{^1H\}$ NMR spectrum of **2** at δ 70.37 (s) and 14.76 (s) while the corresponding peaks for free ether appeared at δ 65.82 and 15.06. The ether ligand did not exchange with CD_2Cl_2 solvent below −60 °C or with free ether at −83 °C on the ^1H NMR time scale.

Isolation and Spectroscopic Characterization of a Dichloromethane Complex. The ether ligand in **2** was tightly bound in the solid state and could not be removed by subjecting the dry powder to a vacuum for several hours, as determined by NMR spectroscopy.[18] It was, however, quite labile in solution as would be expected, and it readily dissociated in methylene chloride solvent. Recrystallization of the cationic platinum species **2** from CH_2Cl_2/hexane at −30 °C led to the isolation of the dichloromethane complex **3** in 80% yield (eq 3). As in

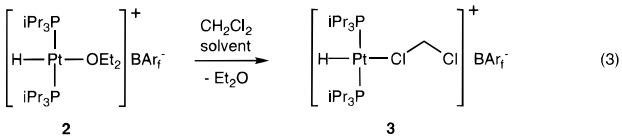

the case of the Et_2O complex **2**, the $^{31}P\{^1H\}$ NMR spectrum of **3** in CD_2Cl_2 at −60 °C contained only a singlet (δ 54.61). The hydride resonance appeared at δ −22.82 (t, J_{HP} = 11.9 Hz, J_{HPt} = 1852 Hz) in the ^1H NMR spectrum. Unfortunately, the resonance for the bound CH_2Cl_2 ligand could not be resolved by $^{13}C\{^1H\}$ NMR spectroscopy. Even at −90 °C in CH_2Cl_2, solvent exchange was rapid on the NMR time scale. When **3** was dissolved in C_6D_5F together with an additional 6 equiv of CH_2Cl_2, the $^{13}C\{^1H\}$ NMR spectrum at −40 °C contained only a sharp singlet at 54.0 ppm for free CH_2Cl_2.

Surprisingly, both **2** and **3** are air stable compounds even in solution. No decomposition or binding of N_2 or O_2 was detected when a solution of **3** in CD_2Cl_2 was saturated with air and then analyzed by NMR spectroscopy. Adventitious water did not coordinate or cause decomposition in this or any other of our experiments. However, H_2O was observed to displace CH_2Cl_2 from **3** when added in nearly 2-fold excess to a CD_2Cl_2 solution in an NMR tube. A new ^{31}P signal appeared at δ 56.69 (J_{PPt} = 2754 Hz) and a broad hydride resonance was seen at δ −26.90 (J_{PtH} = 1644 Hz). In a similar experiment in THF-d_8, the new hydride signal was also broad, indicative of chemical exchange between reversibly-bound ligands. Thus, it is conceivable that exposure of **2** or **3** (or the other weak ligand complexes below) to humid air or wet solvents could result in formation of equilibrium amounts of the presumed H_2O complex, which was not isolated.

The first real evidence that **3** contained a dichloromethane ligand came from IR spectroscopy, which has been shown to be a sensitive probe for binding of CH_2Cl_2 to a metal center.[3,10] The $\nu(CCl)_{asym}$ and $\nu(CCl)_{sym}$ modes for free CH_2Cl_2 dispersed in mineral oil were found at 743 and 707 cm^{-1}, respectively. Upon coordination to the Pt center of **3**, these shifted to 751 and 663 cm^{-1}, respectively. To confirm that these stretches were assigned correctly, the deuterium analog of **3**, $[(PiPr_3)_2Pt(H)(\eta^1\text{-}ClCD_2Cl)]BAr_f$, was prepared by recrystallizing **2** from CD_2Cl_2/hexane at −30 °C. Both of the stretching modes found at 751 and 663 cm^{-1} for **3** were missing from the IR spectrum of the CD_2Cl_2 complex in mineral oil. The spectrum did contain a new band at 643 cm^{-1} assigned to the $\nu(CCl)_{sym}$ stretch, which

(14) (a) Igau, A.; Gladysz, J. A. *Organometallics* **1991**, *10*, 2327. (b) Igau, A.; Gladysz, J. A. *Polyhedron* **1991**, *10*, 1903. (c) Kulawiec, R. J.; Faller, J. W.; Crabtree, R. H. *Organometallics* **1990**, *9*, 745. (d) Winter, C. H.; Veal, W. R.; Garner, C. M.; Arif, A. M.; Gladysz, J. A. *J. Am. Chem. Soc.* **1989**, *111*, 4766. (e) Conroy-Lewis, F. M.; Redhouse, A. D.; Simpson, S. J. *J. Organomet. Chem.* **1989**, *366*, 357. (f) Kulawiec, R. J.; Crabtree, R. H. *Organometallics* **1988**, *7*, 1891. (g) Winter, C. H.; Arif, A. M.; Gladysz, J. A. *J. Am. Chem. Soc.* **1987**, *109*, 7560.

(15) Arndtsen, B. A.; Bergman, R. G. *Science* **1995**, *270*, 1970.

(16) Van Seggen, D. M.; Anderson, O. P.; Strauss, S. H. *Inorg. Chem.* **1992**, *31*, 2987.

(17) (a) Kubas, G. J. *Inorg. Chem.* **1979**, *18*, 182. (b) Ritchey, J. M.; Moody, D. C.; Ryan, R. R. *Inorg. Chem.* **1983**, *22*, 2276.

(18) Although no loss of Et_2O could be detected by NMR spectroscopy when **2** was subjected to a vacuum, the elemental analysis of **2** dried under vacuum overnight indicated that partial loss of Et_2O had taken place.

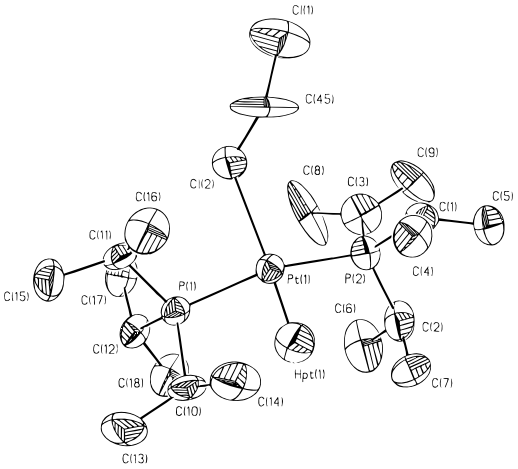

Figure 1. ORTEP diagram of *trans*-$[(PiPr_3)_2Pt(H)(\eta^1\text{-}ClCH_2Cl)]^+$ (**3**), showing the major CH_2Cl_2 binding site (see text).

presumably shifted down 20 cm^{-1} on deuteration because of mode mixing effects. Unfortunately, the $\nu(CCl)_{asym}$ stretch in the CD_2Cl_2 complex was obscured by the BAr_f modes.

Alternate Synthesis of 3. Another convenient preparative route to **3** was found other than that shown in eqs 2 and 3. The reaction of *trans*-$(PiPr_3)_2Pt(H)(Cl)$ with $NaBAr_f$ in CH_2Cl_2 at room temperature led to the isolation of **3** in 63% yield after recrystallization from CH_2Cl_2/hexane at −30 °C (eq 4). The

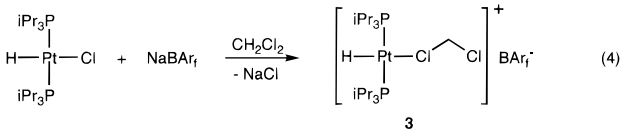

same reaction performed in Et_2O solvent affords the ether complex **2**.

The synthesis of cationic Pt(II) compounds with varying phosphine sizes was also attempted by this method. The reaction of *trans*-$(PEt_3)_2Pt(H)(Cl)$ with $NaBAr_f$ in Et_2O proceeded slowly at room temperature to a mixture of products, indicating that analogues with phosphines with relatively small cone angles are unstable. In contrast, the solvent-free $[(P\text{-}t\text{-}Bu_3)_2Pt(H)]BAr_f$ (see Discussion) was isolated in 64% yield from the reaction of *trans*-$(P\text{-}t\text{-}Bu_3)_2Pt(H)(Cl)$ with $NaBAr_f$ in Et_2O.

X-ray Crystal Structure of $[(PiPr_3)_2Pt(H)(\eta^1\text{-}ClCH_2Cl)]BAr_f$, 3. In order to confirm that methylene chloride was bound to the Pt center as suggested by IR spectroscopy, a crystallographic study was performed on yellow plate-like crystals of **3**. An ORTEP diagram of the cationic portion of the molecule is shown in Figure 1 which clearly shows that CH_2Cl_2 is bound to the Pt center in an η^1-monodentate fashion. Crystal and data collection parameters are given in Table 1, and important bond distances and bond angles are shown in Tables 2 and 3 (an ORTEP diagram of the BAr_f counterion is included in the Supporting Information).

A disordered region near the Pt center was modeled as two disordered CH_2Cl_2 molecules. These two molecules, labeled Cl(2)−C(45)−Cl(1) and Cl(3)−C(45′)−Cl(1), were positioned right next to each other with the outer chloride shared. The two molecules were refined with their site occupancy factors tied to one. In the final refinement the occupancy factors refined to 0.677(8) for the Cl(2)−C(45)−Cl(1) molecule and 0.323(8) for the Cl(3)−C(45′)−Cl(1) molecule. The ORTEP diagram in Figure 1 shows the major site.

For the major CH_2Cl_2 site, the C−Cl(bound) distance was found to be 1.79(2) Å while the C−Cl(unbound) was 1.70(2) Å. Similar distances were observed for the minor CH_2Cl_2 site (C−Cl(bound) = 1.80(4) Å and C−Cl(unbound) = 1.69(4) Å). The Pt−Cl bond length was found to be 2.489(4) Å for the major site and 2.60(1) Å for the minor site. The Cl−C−Cl bond angles were determined to be 111.6(13)° (major site) and 103(2)° (minor site).

Synthesis and NMR Spectroscopic Characterization of the Platinum Haloarene Complexes, 4 and 5. We were surprised to find that the Pt center of **3** could stabilize a dichloromethane ligand, and this prompted us to investigate the scope of reactivity of the unsaturated $[(PiPr_3)_2Pt(H)]BAr_f$ toward other halocarbons. The ether complex **2** reacted with PhI (only 1 equiv is required) at room temperature in methylene chloride to form the colorless air stable PhI complex **4** (eq 5), which was isolated in 87%

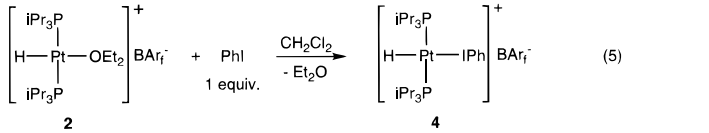

yield by recrystallization from CH_2Cl_2/hexane at −30 °C. The $^{31}P\{^1H\}$ NMR spectrum of **4** in CD_2Cl_2 included only a singlet at δ 53.03, which broadened slightly upon cooling to −93 °C. The hydride resonance appeared in the room temperature ^1H NMR spectrum as a broad resonance at δ −17.02 (J_{HPt} = 1650 Hz) which was resolved as a triplet at −93 °C (δ −15.89, J_{HP} = 9 Hz, J_{HPt} = 1654 Hz). Thus, the overall geometry is the same as that of **2** and **3**.

The ^1H and $^{13}C\{^1H\}$ NMR resonances of PhI are diagnostic of binding in **4**. For example, the ^1H NMR spectrum of free PhI in CD_2Cl_2 contained resonances at δ 7.72 (t, J = 8.4, ortho), 7.36 (t, J = 7.6, para), and 7.13 (vt, J = 7.7, meta) which shifted upon coordination to δ 7.66 (J = 8.1), 7.51 (J = 7.2), and 7.26 (J = 7.6). Similar small shifts were observed in the $^{13}C\{^1H\}$ NMR resonances of PhI. A spectrum of free PhI includes resonances at δ 138.03, 130.85, 128.09, and 94.80 (ipso). The resonances attributed to the PhI ligand of **4** were found at δ 137.21, 131.61, and 130.77. The peak for the ipso carbon in **4** was not resolved and may have been obscured by one of the BAr_f resonances.

Bromobenzene also reacted with the cationic platinum hydride species to form the η^1-aryl halide complex **5**, as shown in eq 6, which was isolated in 60% yield. Whereas only 1 equiv of

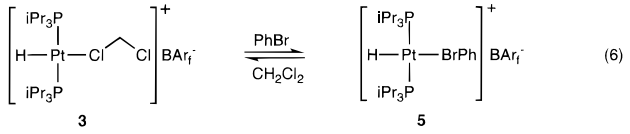

PhI was required to drive the reaction forming **4** to completion, the addition of a large excess of PhBr (ca. 25 equiv) was required in order to observe shifts in the resonances of the dichloromethane complex **3** in CD_2Cl_2. Presumably due to the instability of **5**, the static complex was not resolved by NMR spectroscopy when 5 equiv of PhBr were added to a CD_2Cl_2 solution of **3** even at −90 °C. Rapid ligand exchange also occurred in fluorobenzene. The resonances of PhBr were significantly broadened in the ^1H NMR spectrum of **5** containing an additional 4 equiv of PhBr in C_6D_5F at −40 °C, indicating that the slow exchange regime was being approached (fluorobenzene freezes at −42 °C, preventing further cooling).

As expected, bromobenzene is a weaker ligand than iodobenzene. The following competition experiments were performed in order to gauge relative ligand stabilities. To a CD_2Cl_2 solution of **3** containing 5 equiv of PhBr was added 0.6 equiv

Table 1. Crystal and Data Collection Parameters for **3**, **4**, **5**, **6**, and **7**

	3	**4**	**5**	**6**	**7**
formula weight	1464.71	1583.78	1536.79	2095.34	1451.88
crystal system	monoclinic	triclinic	monoclinic	monoclinic	monoclinic
space group	$P2_1/n$	$P1$	$P2_1/n$	$P2_1/n$	$P2_1/c$
temp (K)	173	173	183	193	173
a (Å)	11.997(2)	12.320(2)	21.142(3)	22.180(4)	11.830(1)
b (Å)	13.067(2)	15.607(1)	12.717(1)	16.383(4)	13.695(1)
c (Å)	37.919(3)	16.993(1)	25.468(2)	25.585(5)	37.657(5)
α (deg)	90	92.2	90	90	90
β (deg)	97.35	106.46	113.503(8)	112.17(1)	99.069(9)
γ (deg)	90	91.09	90	90	90
volume (Å^3)	5895.5(14)	3129.6(6)	6279.5(11)	8610(3)	6025.8(10)
Z	4	2	4	4	4
d_{calc} (g cm^{-3})	1.650	1.681	1.626	1.617	1.600
absp coef (mm^{-1})	2.635	2.893	3.029	3.770	2.493
crystal size (mm)	0.12 × 0.37 × 0.54	0.21 × 0.29 × 0.45	0.16 × 0.21 × 0.37	0.08 × 0.08 × 0.37	0.21 × 0.25 × 0.41
θ range (deg)	2.51−22.50	2.561−25.00	2.51−22.53	2.60−20.00	2.58−22.50
index ranges	$-1 \le h \le 12$	$-1 \le h \le 14$	$-1 \le h \le 22$	$-1 \le h \le 21$	$-21 \le h \le 12$
	$-1 \le k \le 14$	$-1 \le k \le 18$	$-1 \le k \le 13$	$-1 \le k \le 15$	$-1 \le k \le 14$
	$-40 \le l \le 40$	$-20 \le l \le 19$	$-27 \le l \le 25$	$-24 \le l \le 23$	$-13 \le l \le 40$
no. of rflcns collected	9810	6998	9866	9734	9089
no. of indpd reflections	7622	6845	8134	8028	7849
goodness of fit	1.064	0.885	1.022	1.026	1.042
$R(F)$ (%)	4.32	3.85	6.86	7.18	4.73
$R_w(F)$ (%)	9.19	10.11	13.80	13.67	8.69
R_{all} (%)	8.58	5.42	15.47	14.31	10.10

Table 2. Selected Bond Distances (Å) for **3**, **4**, **5**, **6**, and **7**

compd	atom 1	atom 2	distance
3	Pt	P(1)	2.307(2)
	Pt	P(2)	2.310(2)
	Pt	Cl(2)	2.489(4)
	Pt	H(Pt)	1.68(9)
	Cl(1)	C(45)	1.70(2)
	Cl(1)	C(45′)	1.69(4)
	Cl(2)	C(45)	1.79(2)
	Cl(3)	C(45′)	1.80(4)
4	Pt	P(1)	2.311(2)
	Pt	P(2)	2.314(2)
	Pt	I	2.696(1)
	Pt	H(Pt)	1.4(1)
	I	C(1)	2.082(5)
5	Pt	P(1)	2.304(5)
	Pt	P(2)	2.309(5)
	Pt	Br	2.583(2)
	Pt	H(Pt)	1.6(1)
	Br	C(1)	1.91(2)
6	Pt(1)	P(1)	2.302(6)
	Pt(1)	P(2)	2.290(6)
	Pt(2)	P(3)	2.291(6)
	Pt(2)	P(4)	2.300(6)
	Pt(1)	I	2.729(2)
	Pt(2)	I	2.737(2)
	Pt(1)	H(Pt1)	1.6(2)
	Pt(2)	H(Pt2)	1.4(2)
7	Pt	P(1)	2.304(3)
	Pt	P(2)	2.310(3)
	Pt	O	2.224(7)
	Pt	H(Pt)	1.3(1)
	O	C(7)	1.46(1)
	O	C(10)	1.47(1)

Table 3. Selected Bond Angles (deg) for **3**, **4**, **5**, and **6**

compd	atom 1	atom 2	atom 3	angle
3	P(1)	Pt	P(2)	165.77(9)
	P(1)	Pt	Cl(2)	94.03(11)
	P(2)	Pt	Cl(2)	99.50(12)
	Cl(2)	Pt	H(Pt)	178(3)
	C(45)	Cl(2)	Pt	112.1(8)
	C(45′)	Cl(3)	Pt	115(2)
	Cl(1)	C(45)	Cl(2)	111.6(13)
	Cl(1)	C(45′)	Cl(3)	103(2)
4	P(1)	Pt	P(2)	163.75(11)
	P(1)	Pt	I	100.75(7)
	P(2)	Pt	I	95.37(7)
	I	Pt	H(Pt)	170(3)
	Pt	I	C(1)	114.56(19)
5	P(1)	Pt	P(2)	163.89(15)
	P(1)	Pt	Br	102.18(11)
	Br	Pt	H(Pt)	173(5)
	Pt	Br	C(1)	116.4(7)
6	P(1)	Pt(1)	P(2)	168.3(2)
	P(3)	Pt(2)	P(4)	168.9(2)
	Pt(1)	I	Pt(2)	170.14(9)
	P(1)	Pt(1)	I	100.8(2)
	P(2)	Pt(1)	I	90.9(2)
	P(3)	Pt(2)	I	98.6(2)
	P(4)	Pt(2)	I	92.1(2)
	I	Pt(1)	H(Pt1)	171(7)
	I	Pt(2)	H(Pt2)	173(8)
7	P(1)	Pt	P(2)	166.50(11)
	O	Pt	H(Pt)	174(4)
	P(1)	Pt	O	99.3(2)
	P(2)	Pt	O	94.1(2)

of Et_2O. Only one set of resonances was observed by $^{31}P\{^1H\}$ and ^1H NMR spectroscopy at 25 °C. The spectra at −60 °C, however, contained resonances for the Et_2O complex **2** and the rapidly exchanging $PhBr/CD_2Cl_2$ complexes in a ∼5:3 ratio. Thus, all of the ether was bound even in the presence of excess PhBr. In contrast, **4** was stable in Et_2O for 2 days at 90 °C before decomposition could be detected by NMR, although PhI was displaced by THF at room temperature in THF solvent.

Characterization of Haloarene Ligands by Infrared Spectroscopy. As mentioned above, IR spectroscopy has been utilized as a sensitive probe for the ligation of dichloromethane. There are, however, no reports on the effects of transition metal binding on the IR spectra of aryl halides.

The IR (mineral oil) spectrum of the PhI complex **4** was compared with those of the related compounds **2**, **3**, and **5** (discussed below), as well as free PhI, in order to determine which frequencies could be attributed to the iodobenzene ligand. Each band that could be identified was shifted slightly to lower energy relative to those found for free PhI dispersed in mineral oil. For example, bound PhI had peaks at 1569 (Ph), 1011 δ-(CH), 994 υ(Ph), and 652 (Ph) cm^{-1} while those in free PhI appeared at 1573, 1015, 997, and 655 cm^{-1} (spectrometer

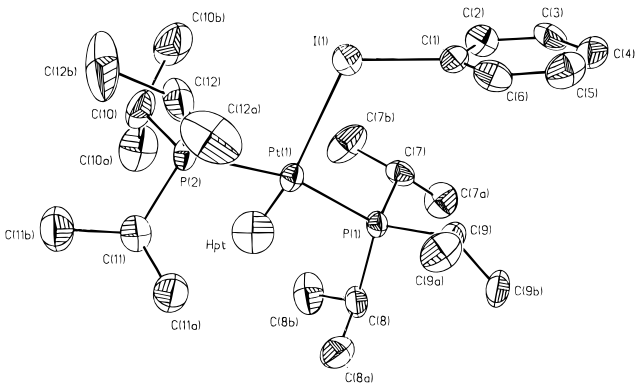

Figure 2. ORTEP diagram of *trans*-$[(PiPr_3)_2Pt(H)(\eta^1\text{-IPh})]^+$ (**4**).

resolution 2 cm^{-1}). The other IR bands expected for bound PhI (and PhBr below), including the C−I stretching vibration, were obscured by the large number of stretching and bending modes of the BAr_f counterion.

The IR (mineral oil) spectrum of **5** contained peaks at 1571 (Ph), 1017 δ(CH), 998 (Ph), and 457 cm^{-1} (Ph) assigned to bound bromobenzene which also only shifted slightly from free PhBr: 1578, 1020, 1000, and 457 cm^{-1}. Although the above studies represent the first report of the effect of ligation on the IR frequencies of an aryl halide, it would appear that, as might be expected, IR is not a sensitive technique for this purpose. Unfortunately, the IR stretch expected to be most affected by the bonding to the Pt center, the C−X stretch, was obscured for both **4** and **5**.

X-ray Crystal Structures of the Iodobenzene and Bromobenzene Platinum Complexes. In order to confirm that **4** and **5** were, in fact, monodentate haloarene complexes rather than the oxidative addition products, X-ray crystallographic studies were performed on both compounds. The ORTEP diagrams of the cationic portions of the molecules, shown in Figures 2 (**4**) and 3 (**5**), show clearly that these are η^1-aryl halide complexes. Crystal and data collection parameters are given in Table 1, and important bond distances and bond angles are shown in Tables 2 and 3.

Both compounds are psuedo-square planar with mutually trans phosphines. The P−Pt−P bond angles in the two compounds were identical (163.7(1)° for **4** and 163.8(1)° for **5**). The Pt−P bond lengths in **4** and **5** were likewise indistinguishable (see Table 2) considering experimental error. The Pt−X bond lengths were found to be 2.696(1) Å where X = I and 2.583(2) Å for X = Br.

Reactivity and Decomposition of Some Halocarbon Complexes: Formation and Structure of a Bridging Iodide Complex, 6. As mentioned in the Introduction, alkyl halide ligands have been shown to be susceptible to nucleophilic attack at the α-carbon much more readily than the free organic halide.[2,14c] The possibility of this reactivity pathway was investigated for the PhI complex **4** as the only halocarbon complex in our study which was stable at room temperature in solution in the sense that it did not exchange with solvent or free PhI on the NMR time scale. In contrast to earlier studies on halocarbon complexes,[2,14c] the PhI ligand of **4** was merely displaced by added nucleophiles. Thus, the addition of L, where L = PPh_3, NEt_3, or Cl^- (added as PPNCl), to **4** at room temperature in methylene chloride quickly produced the corresponding *trans*-$[(PiPr_3)_2Pt(H)(L)]BAr_f$ (or $(PiPr_3)_2Pt(H)(Cl)$ in the case of PPNCl) and free PhI. Not surprisingly, the same observations were made when these nucleophiles were added to the CH_2Cl_2 complex **3** in CD_2Cl_2.

It has been suggested that M(η^1-XR) complexes might represent intermediates in the oxidative addition of alkyl halides

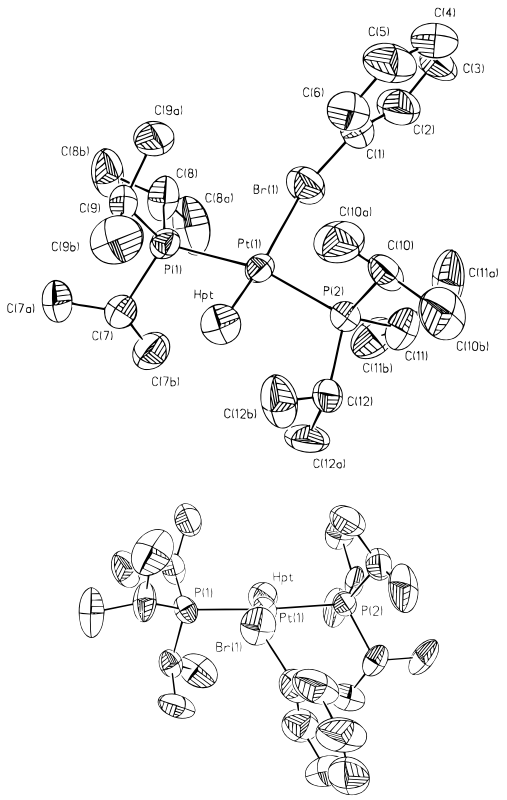

Figure 3. ORTEP diagram of *trans*-$[(PiPr_3)_2Pt(H)(\eta^1\text{-BrPh})]^+$ (**5**): two views of the same molecule.

to metal centers, i.e., they may have relevance in reactions which proceed through an electron transfer mechanism rather than the common S_N2 mechanism.[2,4] Oxidative addition by electron transfer would not be expected for a d^8 Pt(II) species. Thus, it was not surprising that prolonged heating of the PhI complex **4** in CD_2Cl_2 did not lead to the oxidative addition product $[(PiPr_3)_2Pt(H)(Ph)(I)]BAr_f$ but rather slow decomposition to many species (approximately 5% decomposed after 3 days at 80 °C). No benzene was detected in the reaction mixture by NMR spectroscopy. Decomposition was likewise rather slow in Et_2O solvent, requiring 4 days at 100 °C to reach completion. This reaction also did not lead to the oxidative addition product but rather to the air stable bridging iodide complex {*trans*-$[(PiPr_3)_2Pt(H)]_2(\mu\text{-I})\}BAr_f$ (**6**), depicted in eq 7, which was

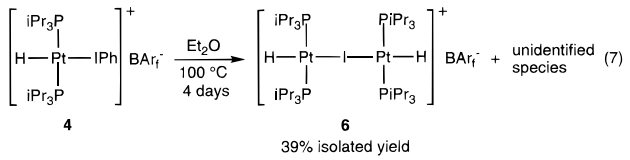

isolated in 39% yield by recrystallization. No other products were observed in this reaction by NMR spectroscopy. The equivalent hydrides of **6** appeared at −18.40 ppm in the ^1H NMR spectrum with a Pt−H coupling constant of 1645 Hz. This is almost identical to the J_{PtH} of 1650 Hz observed in the PhI complex **4**, indicating perhaps that PhI and *trans*-$[(PiPr_3)_2Pt(H)(I)]$ exhibit similar trans influence. The structure of **6** was confirmed by X-ray crystallography (see Figure 4 and Tables 1−3). Both of the formally Pt(II) centers are pseudo-square planar, and the Pt−I−Pt bond angle is almost linear (170.14(9)°). The Pt−I bond lengths are 2.729(3) and 2.737(3) Å. The average Pt−P bond length was found to be 2.296 Å, slightly shorter than the average Pt−P bond distance in **4** (2.312 Å).

Surprisingly, although MeI compounds are more common than aryl iodide complexes,[14] the MeI species *trans*-$[(PiPr_3)_2$-

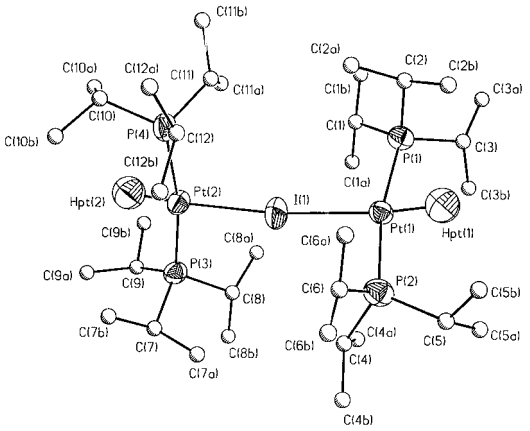

Figure 4. ORTEP diagram of $\{trans\text{-}[(PiPr_3)_2Pt(H)]_2(\mu\text{-}I)\}^+$ (**6**).

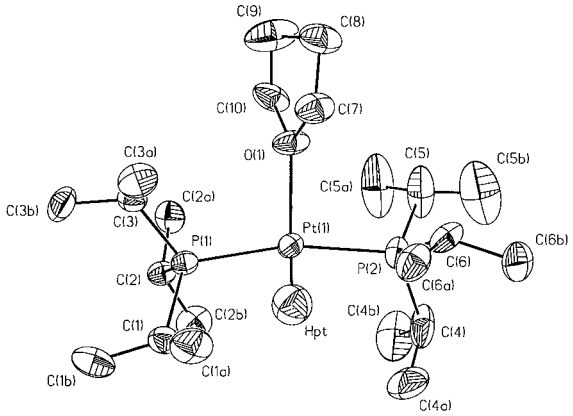

Figure 5. ORTEP diagram of *trans*-$[(PiPr_3)_2Pt(H)(THF)]^+$ (**6**).

Pt(H)(IMe)]BAr_f was much less stable than the PhI compound **4**. When prepared in an NMR tube experiment (15 mg of starting material **3**), the MeI adduct was stable at 25 °C in the presence of excess MeI. When prepared on a large scale, however, the material isolated by recrystallization was a 1:1 mixture of the MeI adduct and **6**. Because the MeI adduct could not be isolated as a pure compound, our evidence that it is a Pt(η^1-IMe) species is circumstantial. Although the halocarbon Me resonance was obscured in the proton NMR spectrum by the phosphine signals, the chemical shifts and shapes of the Pt−H and *i*-Pr resonances were consistent with what was typically observed here for other halocarbon complexes.

Heating the MeI adduct, prepared in situ in Et_2O solvent, for 2.5 h at 65 °C led to the formation of **6** as the only observable product by NMR spectroscopy. As in the case of **4**, the MeI complex decomposed in CD_2Cl_2 (18 h at 70 °C) to a mixture of products, none of which were **6** or the oxidative addition product. Methane, which might have been formed by decomposition of an oxidative addition product, was not detected when the latter reaction was performed in a sealed NMR tube.

Synthesis and Structure of the Pt−THF Adduct, 7. When any of the complexes **2**, **3**, **4**, or **5** were dissolved in THF, the result was displacement of the labile ligand and formation of the air stable THF complex $[(PiPr_3)_2Pt(H)(THF)]BAr_f$ (**7**), which was recrystallized from THF/hexane at −30 °C in 78% yield. The ^1H and $^{31}P\{^1H\}$ NMR spectra of **7** in CD_2Cl_2 were consistent with the same pseudo-square planar geometry assigned to each of the analogous *trans*-$[(PiPr_3)_2Pt(H)(L)]^+$ compounds. The ^1H NMR multiplets for bound THF in **7** (δ 3.84 and 1.94) in CD_2Cl_2 were shifted downfield relative to those for the free ligand (3.68 and 1.82 ppm). Similarly, at −10 °C in CD_2Cl_2, the bound THF gave rise to ^{13}C NMR resonances at δ 74.38 and 25.60 while those for free THF appeared at δ 68.11 and 25.91.

Complex **7** was also characterized by X-ray crystallography, which surprisingly represents the first structural determination of an unsupported THF complex of platinum (see Figure 5 and Tables 1−3). The Pt−O distance was found to be 2.224(7) Å. This is substantially longer than the Pt−O distance of 2.142(4) Å found in a related Pt(II) complex in which a THF ligand was stabilized by phosphine chelation.[19] The C−O bond distances of 1.46(1) and 1.47(1) Å in **7** are consistent with those of the above chelate complex as well as unsupported THF complexes of other transition metals.[20]

Reactivity of the CH_2Cl_2 Complex toward Dihydrogen. As part of the continued interest in the coordination of H_2 to transition metal complexes,[21] we were curious as to whether H_2 would form a stable complex with the unsaturated *trans*-$[(PiPr_3)_2Pt(H)]BAr_f$ and how it would compete as a ligand with CH_2Cl_2. Thus, approximately three atmospheres of H_2 were added to a yellow CD_2Cl_2 solution of **3**. The room temperature ^1H NMR spectrum contained no resonances for free H_2 or the Pt−H, indicating that a fluxional process was taking place. At −60 °C, however, the ^1H NMR spectrum contained a sharp singlet at 4.55 ppm, a broad lump at δ 0.36, and a triplet at −10.13 (J_{HP} = 9.9, J_{HPt} = 1438 Hz). These resonances are assigned to free H_2 and the dihydrogen ligand and hydride, respectively, of the dihydrogen complex *trans*-$[(PiPr_3)_2Pt(H)(H_2)]BAr_f$ (**8**) shown in eq 8. Each of these three resonances

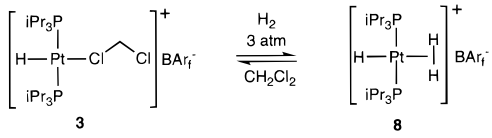

(8)

broadened into the baseline upon rewarming between −10 °C and 0 °C. The $^{31}P\{^1H\}$ NMR spectrum at −60 °C included only a singlet at δ 57.58 (J_{PPt} = 2432 Hz) which was not observed at this temperature in the absence of H_2. The HD coupling constant for the HD isotopomer of **8** was found to be 33.7 Hz at −80 °C, while that for free HD is 42.6 Hz at this temperature. In general, J_{HD} values for M(η^2-HD) compounds are found between 9 and 35 Hz depending on the degree of metal-to-ligand back-bonding.[21] The high value here suggests an H-H distance in the "short" range, 0.8−0.9 Å, typical of unactivated dihydrogen ligands. As found for $[Mn(CO)(Ph_2PC_2H_4PPh_2)_2(H_2)]BAr_f$[22] and other cationic systems,[21] the positive charge on the metal undoubtedly helps to stabilize sigma coordination rather than oxidative addition of H_2. The positioning *trans* to hydride in **8** also contributes to the high lability of the H_2 ligand because of the *trans* effect. No exchange between

(19) Alcock, N. W.; Platt, A. W. G.; Pringle, P. G. *J. Chem. Soc., Dalton Trans.* **1989**, 2069.

(20) See, for example: (a) Dick, D. G.; Stephan, D. W. *Organometallics* **1990**, *9*, 1910. (b) Davies, C. E.; Gardines, I. M.; Green, J. C.; Green, M. L. H.; Hazel, N. J.; Grebenik, P. D.; Mtetwa, V. S. B.; Prout, K. *J. Chem. Soc., Dalton Trans.* **1985**, 669. (c) Churchill, M. R.; Wasserman, H. J. *Inorg. Chem.* **1982**, *21*, 223. (d) Cotton, F. A.; Lewis, G. F.; Mott, G. N. *Inorg. Chem.* **1982**, *21*, 3127.

(21) (a) Heinekey, D. M.; Oldham, W. J., Jr. *Chem. Rev.* **1993**, *93*, 913. (b) Jessop, P. G.; Morris, R. H. *Coord. Chem. Rev.* **1992,** *121*, 155. (c) Crabtree, R. H. *Acc. Chem. Res.* **1990**, *23*, 95. (d) Kubas, G. J. *Acc. Chem. Res*. **1988**, *21* , 120.

(22) King, W. A.; Luo, X.-L.; Scott, B. L.; Kubas, G. J.; Zilm, K. *J. Am. Chem. Soc*. **1996**, *118*, 6782.

deuterium from HD or D_2 and the Pt−hydride took place when samples under these gases were warmed to room temperature for 20 min and then reanalyzed by NMR spectroscopy at −80 °C.

Our findings are analogous to those recently reported by Gusev and Caulton for a closely related compound.[23] These workers treated *trans*-(P-*t*-$Bu_3)_2Pt(H)_2$ with triflic acid to form the dihydrogen complex *trans*-[(P-*t*-$Bu_3)_2Pt(H)(H_2)$]OTf stable only at low temperature. This complex had ^{1}H NMR resonances (δ_{HH} 1.12, J_{HD} = 34.7 Hz) and exhibited temperature dependent behavior quite similar to that observed for **8**.

Discussion

Synthesis of a Highly Reactive Cationic Platinum Species: A Precursor to Alkyl and Aryl Halide Complexes. The reaction of $Pt(PiPr_3)_3$ with SO_2 in ether led to the loss of one $PiPr_3$ and the isolation of $(PiPr_3)_2Pt(SO_2)$ (**1**) (eq 1), which reacted with $HBAr_f$ in ether to give clean formation of the solvent species *trans*-[$(PiPr_3)_2Pt(H)(OEt_2)$]BAr_f (**2**, eq 2). A likely mechanism for the reaction forming **2** is shown in eq 9.

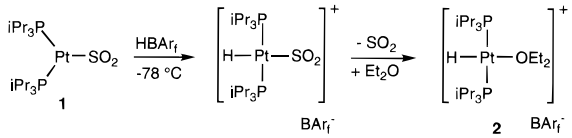

(9)

The first step in this mechanism is the protonation of the platinum center to form the four-coordinate SO_2 complex. The facile loss of SO_2 from this cationic Pt species followed by the binding of a solvent molecule affords the observed product. The reaction might also proceed through a sulfinic acid species, $[(PiPr_3)_2Pt(SO_2H)]^+$, either from direct protonation at SO_2 or as a tautomer[24] of the intermediate in eq 9. If a Pt−sulfinic acid species were stable at −78 °C, we would expect it to be deprotonated by added base to reform starting material. To test this, **1** was treated with 1 equiv of $HBAr_f$ at −78 °C followed 8 min later by 2 equiv of NEt_3 (the delay ensured that all $HBAr_f$ was consumed by reaction with **1**). Only **2** was observed by NMR when the reaction mixture was warmed to room temperature, pumped dry, and dissolved in CD_2Cl_2. Likewise no starting material was observed when the much stronger base *n*-BuLi was substituted for NEt_3 (unidentified species resulted). Regardless of reaction pathway, these and other observations suggest that SO_2 is rapidly and irreversibly lost on acid addition even at −78 °C.

Although another convenient route to **2** was found (eq 4, in Et_2O solvent), the reaction shown in eq 2 is important in part because it illustrates the versatility of the SO_2 ligand. The SO_2 group, which was strongly bound in the neutral starting material $(PiPr_3)_2Pt(SO_2)$ (**1**), became exceptionally labile upon protonation of the compound with $HBAr_f$, and even a large excess of SO_2 would not replace the weakly bound ether in **2**. Just as for metal-to-carbon back-donation in carbonyl complexes, metal-to-sulfur back-bonding has been shown to be important in the stabilization of SO_2 ligands.[25] We suggest then that the observed lability of SO_2 in the reaction of eq 2 is a result of the drastically decreased back-bonding ability of cationic Pt(II) vs Pt(0).

Interestingly, the ether complex **2** could not be synthesized by allowing $HBAr_f$ to react directly with $Pt(PiPr_3)_3$ rather than **1**, despite the ease with which the tris(phosphine) compound dissociates phosphine in solution and the obvious steric advantages of replacement of bulky $PiPr_3$ by solvent. This reaction yielded only the cationic tris(phosphine)−Pt−hydride species shown in eq 10,[26] reiterating the exceptional lability of SO_2 on Pt(II).

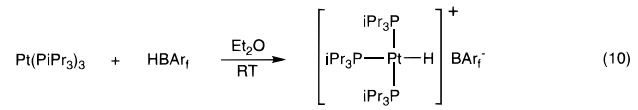

(10)

Successful isolation of the cationic Pt ether complex **2** required the utilization of a large, low coordinating anion such as BAr_f^-. Smaller, more nucleophilic anions functioned as ligands which were not displaced by halocarbons. For example, the addition of triflic acid to **1** in ether at −78 °C led only to *trans*-$(PiPr_3)_2Pt(H)(OTf)$.

Synthesis and Solution Behavior of [$(PiPr_3)_2Pt(H)(\eta^1$-$ClCH_2Cl)$]BAr_f, 3. Recrystallization of [$(PiPr_3)_2Pt(H)(OEt_2)$]BAr_f (**2**) from CH_2Cl_2/hexane led to the isolation of the methylene chloride complex **3** (eq 3). The CH_2Cl_2 ligand in **3** is so labile in solution that the static complex was not observed even at −90 °C in CH_2Cl_2 by $^{13}C\{^1H\}$ NMR spectroscopy. Compound **3** was then dissolved in C_6D_5F together with an additional 6 equiv of CH_2Cl_2. Only one resonance was observed for CH_2Cl_2 in both the ^{1}H and $^{13}C\{^1H\}$ NMR spectra at −40 °C, and these were unshifted from those observed under the same conditions in the absence of **3**. We believe that rapid solvent exchange on the NMR time scale, even in fluorobenzene, is consistent with these results. In contrast to the behavior of **3**, the $^{13}C\{^1H\}$ NMR resonances for the CH_2Cl_2 ligands in the compounds $[(C_5R_5)Re(PPh_3)(NO)(CH_2Cl_2)]BF_4$ (R = H, Me) were identified at −85 °C.[27,28]

While our results may be in agreement with the persistence of the coordinatively unsaturated $[(PiPr_3)_2Pt(H)]BAr_f$ species in solution, this is highly unlikely. A strong argument against this is the fact that this unsaturated species can be isolated as the methylene chloride adduct in the solid state. Furthermore, the Pt−H coupling constant (1852 Hz at −60 °C) of **3** in CD_2Cl_2 is significantly smaller than what might be expected in the absence of a ligand *trans* to the hydride. The more sterically bulky complex [(P-*t*-$Bu_3)_2Pt(H)]BAr_f$, prepared in the reaction of *trans*-(P-*t*-$Bu_3)_2Pt(H)(Cl)$ with $NaBAr_f$, did not react with an excess of either PhI or MeI at 25 °C. This compound is believed to indeed exist as a 3-coordinate complex in CD_2Cl_2, and importantly has a much larger J_{HPt} of 2605 Hz at room temperature. Consistent with our results, the series of closely related 3-coordinate compounds [(P-*t*-$Bu_3)_2Pt(H)]X$ (where X = BF_4, PF_6, ClO_4, SO_3CF_3) previously studied by Goel and coworkers gave a Pt−H coupling constant of 2570 Hz invariant to the nature of X.[29] The binding of a number of ligands (H_2O, acetone, MeCN, etc., but not CH_2Cl_2) trans to the hydride led to a decrease in J_{PtH} on the order of 1000−1100 Hz. Thus, our

(23) Gusev, D. G.; Notheis, J. U.; Rambo, J. R.; Hauger, B. E.; Eisenstein, O.; Caulton, K. G. *J. Am. Chem. Soc.* **1994**, *116*, 7409.

(24) For known SO_2H complexes, see: (a) Kubas, G. J.; Wasserman, H. J.; Ryan, R. R. *Organometallics* **1985**, *4*, 2012. (b) Randall, S. L.; Miller, C. A.; Janik, T. S.; Churchill, M. R.; Atwood, J. D. *Organometallics* **1994**, 13, 141.

(25) Ryan, R. R.; Kubas, G. J.; Moody, D. C.; Eller, P. G. *Struct. Bonding (Berlin)* **1981**, *46*, 47.

(26) This complex was not prepared on a large scale but was readily identified by NMR spectroscopy: ^{1}H NMR (THF-d_8) δ 7.79 (s, 8H, BAr_f), 7.57 (s, 4H, BAr_f), 2.61 (m, 6H, CH), 2.54 (m, 3H, CH), 1.42 (dd, J = 13.8 and 7.2, 18H, CH_3), 1.33 (vq, J = 7.2, 36H, CH_3), −9.12 (dt, J_{HP} = 145.0 and 17.1, J_{HPt} = 634, 1H, PtH); $^{31}P\{^1H\}$ NMR (THF-d_8) δ 41.82 (d, J_{PP} = 18.3, J_{PPt} = 2585), 39.66 (t, J_{PP} = 18.3, J_{PPt} = 2391).

(27) (a) Fernandez, J. M.; Gladysz, J. A. *Organometallics* **1989**, *8*, 207. (b) Winter, C. H.; Arif, A. M.; Gladysz, J. A. *Organometallics* **1989**, *8*, 219.

(28) Peng, T. -S.; Winter, C. H.; Gladysz, J. A. *Inorg. Chem.* **1994**, *33*, 2534.

(29) Goel, R. G.; Srivastava, R. C. *Can. J. Chem.* **1983**, *61*, 1352.

Table 4. Platinum−Hydride Coupling Constants for *trans*-[$(PiPr_3)_2Pt(H)(L)BAr_f$

L	J_{Pt-H} (Hz)	L	J_{Pt-H} (Hz)	L	J_{Pt-H} (Hz)
CH_2Cl_2	1852[a]	Et_2O	1540	Et_3N	1359
PhBr	1781[b]	THF	1507	Cl^-	1280[c]
PhI	1654	H_2	1438	PPh_3	784[c]
MeI	1631	I^-	1363[c]		

[a] Ligand exchange averaged value in CD_2Cl_2 solvent at −60 °C. [b] Ligand exchange averaged value when 5 equiv of PhBr was added to a CD_2Cl_2 solution at −80 °C. [c] For these compounds the ligand L was added to a CD_2Cl_2 solution of **3**; they were not isolated.

observation of a J_{HPt} of 1852 Hz is consistent with the existence of a weakly bound ligand, such as CH_2Cl_2, trans to the hydride.

It is interesting to compare J_{HPt} for a series of complexes of the type *trans*-[$(PiPr_3)_2Pt(H)(L)]BAr_f$ (Table 4). There seems to be a rough inverse correlation with ligand binding strengths, although there are exceptions. For example, PhI is a better ligand than Et_2O in the sense that it does not dissociate from **4** in Et_2O solvent, but it has a larger J_{HPt}. Another notable exception is the H_2 complex **8**, which had a J_{HPt} of 1438 Hz at −60 °C. This relatively small coupling would seem to imply that H_2 is a much stronger ligand than demonstrated by our variable temperature NMR studies (see Results). However, dihydrogen is the only ligand in the series which can function as a good π-acceptor (see discussion below regarding π bonding in **4**), and it is possible that Pt → H_2 back-bonding has the effect of lowering the J_{PtH} of the *trans*-hydride.

X-ray Crystal Structure of [$(PiPr_3)_2Pt(H)(\eta^1$-$ClCH_2Cl)]BAr_f$. The geometry about the Pt center is pseudo-square planar, and the phosphine ligands are trans to one another as expected from the NMR spectroscopic studies (P−Pt−P = 165.77(9)°). Because of the experimental error in the bond lengths and angles of the coordinated CH_2Cl_2 molecule, a clear analysis of the effects of Pt−Cl bonding on these values is prohibited. They are, in any case, comparable to the values reported for free CH_2Cl_2 in the gas phase (C−Cl = 1.7724(5) Å and Cl−C−Cl = 111.78(2)°).[30] The Pt−Cl distance of 2.489(4) Å found for the major CH_2Cl_2 site is longer than that found in the chelating halocarbon complex [MePt{η^2-$Ph_2P(CH_2CH_2Cl)$}{η^1-$Ph_2P(CH_2CH_2Cl)$}]BF_4 (2.425(1) Å)[9c] as well as what is normally observed for terminal Pt(II)−Cl bonds. For example, the analogous neutral compound *trans*-$(PiPr_3)_2Pt(H)(Cl)$ had a Pt−Cl distance of 2.395(1) Å.[31] The elongation of this bond in **3** is consistent with the observed lability of the methylene chloride ligand in solution.

While a few complexes containing bidentate CH_2Cl_2 or 1,2-$C_2H_4Cl_2$ ligands have been characterized by X-ray,[10,11,12] there is only one other example of a structurally characterized monodentate CH_2Cl_2 complex. Recently, Arndtsen and Bergman reported the structure of Cp*Ir$(PMe_3)(Me)(\eta^1$-$ClCH_2Cl)]BAr_f$ which had CH_2Cl_2 bond distances and angles consistent with those of **3**.[15] A longer chain RCl−Ag interaction has been structurally characterized by Strauss and co-workers in [Ag-$(1,2,3\text{-}C_3H_5Cl_3)OTeF_5]_2$ which contains a trichloropropane ligand bound through only one chloride.[16]

Synthesis and Stability of the Haloarene Complexes [$(PiPr_3)_2Pt(H)(\eta^1$-XPh)]BAr_f, 4 and 5. The unsaturated fragment $[(PiPr_3)_2Pt(H)]^+$ could be stabilized by halocarbon ligands other than methylene chloride. Both the iodo- and bromobenzene complexes **4** and **5** were isolated from the reaction of either the ether complex or the CH_2Cl_2 complex with PhX in CH_2Cl_2 (eqs 5 and 6). Aryl iodide complexes such as **4** are quite scarce compared to those of alkyl iodides. The isolable η^1-iodobenzene complex [CpRe(NO)(PPh_3)(IPh)]BF_4 has been reported.[14d] The complex $[H_2Ir(PPh_3)_2(IPh)_2]BF_4$ reportedly existed at −60 °C but was unstable and could not be isolated.[4] The more basic aryl halides 4-iodoanisole and 4-iodotoluene have formed the isolable complexes [CpRe(NO)(PPh_3)(p-IC_6H_4OMe)]BF_4[14d] and [CpRu(CO)(PPh_3)(p-IC_6H_4Me)]BF_4.[14c]

As expected, the PhBr complex **5** was much less stable than that of PhI and represents the first example of an *isolable* complex containing a monodentate organic bromide ligand.[32] The EtBr compound [CpRe(NO)(PPh_3)(BrEt)]BF_4 was characterized at low temperature by NMR spectroscopy by Gladysz and co-workers but was unstable.[14d]

Solid State Structure of [$(PiPr_3)_2Pt(H)(\eta^1$-IPh)]BAr_f, 4. A crystallographic study confirmed that **4** was a monodentate haloarene compound (see Figure 2 and Tables 1−3). The Pt−I bond length of 2.696(1) Å is at the upper end of the range normally found for terminal Pt−I bond distances in other Pt(II) compounds (approximately 2.60−2.70 Å).[33] The only other structurally characterized organic iodide complex of Pt is the chelating compound *cis*-$(C_6F_5)_2Pt(N-I)$, where N−I is 2-iodoaniline, which had a Pt−I distance of 2.620(1) Å.[7]

The Pt−I−C(1) angle of 114.56(19)° is larger than would be expected compared to other monodentate halocarbon compounds; M−X−C angles are usually found in the 100−110° range.[5,14c−e] These acute angles have been rationalized by characterizing the donor orbital on the halide as having a significant amount of p character (little s−p mixing), an explanation which is consistent with theoretical calculations on $L_nM(\eta^1$-XR) compounds.[34,35] For example, Hoffmann predicted a Pt−I−C angle of 100° in model compound $Pt(Ph)(NH_3)_2(IMe)^+$.[34]

The most unusual feature of the structure of the PhI complex **4**, and most likely the reason for the larger than expected Pt−I−C(1) angle, is the orientation of the phenyl group, which is situated over one of the phosphine isopropyl groups as a result of a small C(1)−I−Pt−P(1) dihedral angle of −19.8°. This can be easily seen in the ball and stick drawings shown in Figure 6. The phenyl ring lies essentially flat over the phosphine, with a C(6)−C(1)−I−Pt dihedral angle of −87.6°. Analysis of a space filling model of **4** suggested that in consideration of sterics alone, the phenyl ring should lie above or below the plane of the molecule, between the two phosphines (i.e., with a much larger C(1)−I−Pt−P(1) dihedral angle), as observed in the structure of the related compound $(PEt_3)_2Pt(H)(OPh)$.[36] Significantly, there are no close contacts between the iodide and any hydrogens on the phosphines (the shortest I···H distance is 2.986 Å) or between neighboring molecules.

Molecular Mechanics Calculations on [$(PiPr_3)_2Pt(H)(\eta^1$-IPh)]$^+$. An important question is, therefore, the following. Does the geometry adopted by **4** in the solid state as shown in Figure 2 really include a significant steric repulsion between the phenyl and isopropyl groups, or could these observations simply be the result of crystal packing forces? In order to probe the sterics more indepth, molecular modeling calculations were performed

(30) Myers, R. J.; Gwinn, W. D. *J. Chem. Phys.* **1952**, *20*, 1420.
(31) Robertson, G. B.; Tucker, P. A.; Wickramasinghe, W. A. *Aust. J. Chem.* **1986**, *39*, 1495.
(32) Structures of complexes containing chelating M···Br interactions have, however, been reported. See ref 8.
(33) (a) Boag, N. M.; Rao, K. M.; Terrill, N. J. *Acta Crystallogr., C* **1991**, *47*, 1064. (b) Ogawa, H.; Onitsuka, K.; Joh, T.; Takahashi, S.; Yamamoto, Y.; Yamazaki, H. *Organometallics* **1988**, *7*, 2257. (c) Manojlovic-Muir, L.; Ling, S. S. M.; Puddephatt, R. J. *J. Chem. Soc., Dalton Trans.* **1986**, 151. (d) Hunter, W. N.; Muir, K. W.; Sharp, W. A. *Acta Crystallogr., C* **1986**, *42*, 1743.
(34) Ortiz, J. V.; Havlas, Z.; Hoffmann, R. *Helv. Chim. Acta* **1984**, *67*, 1.
(35) Czech, P. T.; Gladysz, J. A.; Fenske, R. F. *Organometallics* **1989**, *8*, 1806.
(36) Cowan, R. L.; Trogler, W. C. *J. Am. Chem. Soc.* **1989**, *111*, 4750.

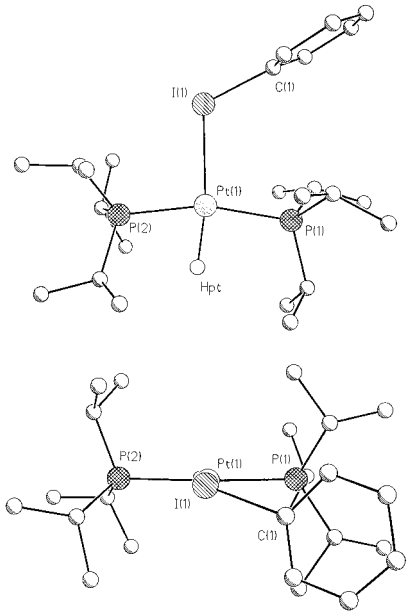

Figure 6. Ball and stick diagrams of *trans*-$[(PiPr_3)_2Pt(H)(\eta^1\text{-IPh})]^+$ (**4**).

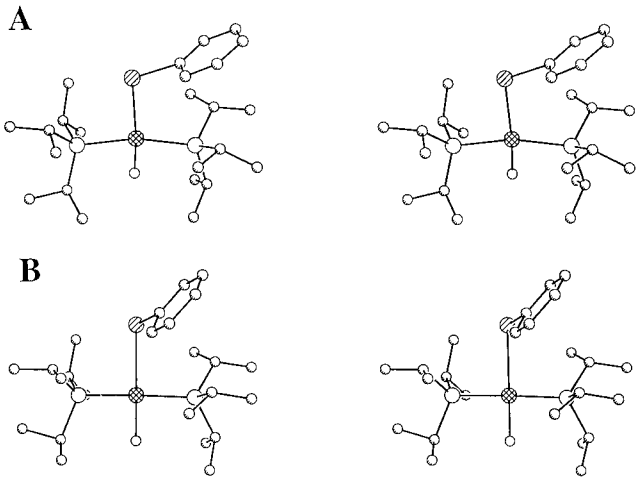

Figure 7. Molecular mechanics calculations on *trans*-$[(PiPr_3)_2Pt(H)(\eta^1\text{-IPh})]^+$ (**4**): (A) stereoview of the starting structure, derived from the crystal structure coordinates, (B) stereoview of the optimized geometry of the platinum cation.

on the cationic portion of **4** using the ESFF force field within Discover 95.0.[37]

The atomic coordinates of **4**, with the hydride ligand replaced by a fluoride at the default distance of 1.623 Å (see the Experimental Section), were used to generate the starting structure shown in Figure 7A. Optimization led to the structure shown in Figure 7B. The initial and final energies were 61.87 and 51.42 kcal, respectively. The results of bond distance and angle optimization are summarized in Table 5. As can be seen in the stereoviews of Figure 7, the steric strain of having the phenyl ring in close proximity to the isopropyl groups was relieved in essentially three ways: (1) rotation about the Pt−I bond thus decreasing the C(1)−I−Pt−P(1) dihedral angle from −19.8° to −58.3°, (2) rotation about the I−C(1) bond such that the C(6)−C(1)−I−Pt dihedral angle is increased from −87.6° to −47.4°, and (3) optimizing the orientation of the phosphine ligand close to the phenyl group in structure A. While the substitution of a fluoride ligand for the hydride probably has some small effect on the determination of a 10.45 kcal energy

(37) Discover 95.0 is a product of Molecular Simulations Inc., 9685 Scranton Rd., San Diego, CA 92121-3752.

Table 5. Molecular Mechanics Calculations on *trans*-$[(PiPr_3)_2Pt(H)(\eta_1\text{-IPh})]^+$: Important Structural Parameters Initial and Minimized Structures[a]

dihedral angle	initial (deg)	minimized (deg)
C(1)−I(1)−Pt(1)−P1	−19.8	−58.3
Pt(1)−P(1)−C(9)−C(9a)	31.1	41.6
C(6)−C(1)−I(1)−Pt(1)	−87.6	−47.4
Pt(1)−P(1)−C(7)−C(7b)	−39.1	−33.0
I(1)−Pt(1)−P(1)−C(7)	−57.9	−50.3
I(1)−Pt(1)−P(1)−C(9)	59.0	67.2
Pt(1)−P(1)−C(7)−H(7)	74.7	82.4
Pt(1)−P(1)−C(9)−H(9)	−84.6	−72.3
bond angle	**initial (deg)**	**minimized (deg)**
Pt(1)−I(1)−C(1)	114.8	113.7
C(7)−P(1)−C(9)	104.3	105.0
P(2)−Pt(1)−P(1)	163.8	176.4
I(1)−Pt(1)−P(1)	100.8	90.9
I(1)−Pt(1)−P(2)	95.4	91.8
I(1)−Pt(1)−F	170.3	179.9
bond distance	**initial (Å)**	**minimized (Å)**
Pt(1)−I(1)	2.696	2.836
Pt(1)−P(1)	2.311	2.305
Pt(1)−P(2)	2.314	2.301
I(1)−C(1)	2.123	2.095
Pt(1)−F	1.623	1.874

[a] Distances and Angles refer to Figure 7.

difference between structures A and B, we believe that these calculations serve to show, overall, that (a) **4** in the solid state does contain a significant steric interaction between the phenyl and isopropyl groups and (b) this interaction is too energetically unfavorable to have come about by crystal packing forces.

Halide-to-Metal π Bonding in $[(PiPr_3)_2Pt(H)(\eta^1\text{-IPh})]^+$. In light of these results, we next looked for electronic reasons for the observed solid state geometry of **4**. We believe that the orientation of the iodobenzene ligand of **4** is consistent with invoking π donation from the iodide to the Pt center. The interaction between a planar ML_3 fragment and the lone pair p orbitals on iodide is considered in the MO diagram shown in Figure 8. The Pt−I single bond results from the interaction of the lone pair in the p_y orbital of iodide with the empty $2a_1$ metal-based orbital. We propose that the lone pair in the iodide p_z orbital overlaps with the metal d_{yz} and p_z orbitals to form a π bond. Π overlap between the iodide lone pair and the Pt d_{yz} orbital is a filled−filled interaction, and it is mixing with the empty Pt p_z orbital that makes it overall bonding. In this scenario, the stabilization gained in Pt p_z mixing is qualitatively sufficient to outweigh the steric repulsion between the phenyl and isopropyl groups.

This type of π bonding would also be allowed by symmetry if the phenyl ring as shown in Figure 6 was rotated approximately 90° about the Pt−I bond such that it lay above or below the plane of the molecule. However, stabilization of the corresponding pπ−dπ filled−filled interaction could only be provided by mixing with the Pt p_x orbital. While the Pt p_z orbital in the ML_3 fragment is nonbonding, the Pt p_x orbital is antibonding and is most likely too high in energy to stabilize a Pt−I π interaction.

The idea of π bonding between terminal halides and transition metals has been around for a long time,[38] and numerous recent studies by Caulton and Eisenstein have substantiated the existence of π interactions in organometallic M−X (X = halide, alkoxide) compounds.[39] The present work shows that such π bonding may exist even when the halide is bound to an organic

(38) (a) Jolly, W. L. *J. Phys. Chem.* **1983**, *87*, 26. (b) Hall, M. B.; Fenske, R. F. *Inorg. Chem.* **1972**, *11*, 1619.

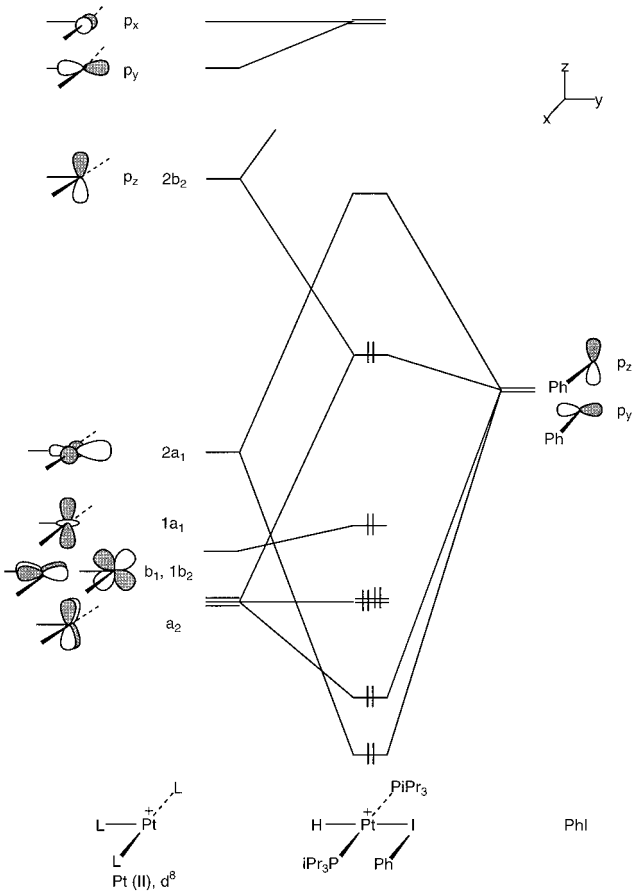

Figure 8. Molecular orbital diagram of *trans*-$[(PiPr_3)_2Pt(H)(\eta^1\text{-IPh})]^+$ (**4**).

moiety. More advanced calculations on our Pt system are clearly called for, but our results thus far would suggest that the overall stabilization afforded to **4** by the existence of a Pt−I π bond is at least 10 kcal. Π bonding, as described herein, has not previously been suggested to exist in halocarbon compounds.

It has been concluded by many workers that π bonding does not occur to any significant extent in square planar Pt(II) alkoxide, hydroxide, or amide complexes.[36,39c,40] This is because π interactions in such compounds are repulsive if one does not consider the participation of the empty Pt p_z orbital to be significant. We do not doubt that this is a reasonable assumption with OR, OH, and NR_2 ligands. However, the lone pairs on iodide (as RI) exist at higher energy than do those on OR, OH, and NR_2 ligands, and are perhaps better suited for interactions with Pt(II) p and d orbitals.[34] Furthermore, the participation of the Pt(II) p_z orbital in ligand substitution reactions of square planar compounds has been widely recognized.[41]

In principle, ligands of the type $M(\eta^1\text{-XR})$ can act as π acceptors.[5,27,42] Because of the small M−X−C bond angles typically observed in halocarbon compounds, the empty C−X σ^* orbital can overlap with a filled metal d orbital. In the case of the PhI complex **4**, such an interaction is no more favored in the observed geometry (Figure 6) than it would be in the less sterically hindered structure in which the phenyl ring is rotated about the Pt−I bond by 90°. This type of back-bonding has also been found to be insignificant in other systems as well.[35]

Low Temperature NMR Spectroscopy of $[(PiPr_3)_2Pt(H)(\eta^1\text{-IPh})]BAr_f$. As shown in our crystallographic study, in the solid state the two phosphines of **4** are chemically inequivalent (Figures 2 and 6). In solution, however, only one resonance (slightly broadened) was observed for the two phosphines by $^{31}P\{^1H\}$ NMR spectroscopy even at −80 °C in CD_2Cl_2, unshifted from that observed at room temperature. The chemical inequivalence between the phosphines in the static compound would be expected to be largely due to the ring current of the phenyl group over one phosphine and not the other. Because the temperature at which the two resonances can be resolved depends, of course, on the chemical shift difference between them in the slow exchange regime, it seems most likely that this shift is too small to be resolved at −80 °C.

Interestingly, the resonances for the averaged isopropyl CH and CH_3 groups for the PhI complex **4** (2.30 ppm, CH; 1.24 ppm, CH_3) were found downfield of those for the exchange averaged (see the Experimental Section) isopropyl resonances for **3** in the presence of seven equivalents of bromobenzene (2.24 ppm, CH; 1.19 ppm, CH_3). It is possible that these observations are the result of deshielding in the case of **4**, wherein the phenyl ring lies over the isopropyl groups to a greater extent in solution compared to the PhBr complex **5**.

X-ray structure of $[(PiPr_3)_2Pt(H)(\eta^1\text{-BrPh})]BAr_f$, 5. In order to compare the structure of the bromobenzene complex with that of iodobenzene, an X-ray crystallographic study of **5** was performed on crystals isolated from a CH_2Cl_2 solution of **3** containing 25 equiv of PhBr at −30 °C (Figure 3). There are important structural differences between the PhBr and PhI compounds. Unlike in **4**, the phenyl ring of **5** is not situated over one of the phosphine isopropyl groups. Rather it adopts a geometry like the optimized structure of **4** shown in Figure 7B. More specifically, the C(1)−Br−Pt−P(2) dihedral angle of −56.4° in **5** is much closer to that found for the optimized structure of **4** (Figure 7B, Table 5, −58.3°) than for **4** itself (−19.8°). Likewise, the C(6)−C(1)−Br−Pt dihedral angle of −30.0° compares more favorably with that in the optimized **4** (−47.4°) than with the analogous angle of −87.6° determined from the crystal structure of **4**. The differences between the structures of **4** and **5** are most likely caused by steric interactions. The Pt−Br distance in **5** is shorter than the Pt−I distance in **4** (2.583(2) vs 2.696(1) Å) and requires that the phenyl ring be closer within the coordination sphere of the platinum center in **5** and thus closer to the phosphine isopropyl groups. The geometry requirement for π bonding as described for **5** in Figure 8 is thus broken, but because it is possible that hybridization at Br could allow for π bonding in other PhBr orientations, it is not clear whether or not Pt−Br π bonding exists in **5**. The Pt−Br bond length of 2.583(2) Å is near the upper limit of the range normally found for Pt−Br bonds (2.43−2.60 Å)[43,44] and is consistent with the characterization of this bond as a relatively weak one.

Formation and Structure of $\{$*trans*-$[(PiPr_3)_2Pt(H)]_2(\mu\text{-I})\}$-$BAr_f$ (6). Despite the propensity for organic iodides to

(39) (a) Gusev, D. G.; Kuhlman, R.; Rambo, J. R.; Berke, H.; Eisenstein, O.; Caulton, K. G. *J. Am. Chem. Soc.* **1995**, *117*, 281. (b) Johnson, T. J.; Folting, K.; Streib, W. E.; Martin, J. D.; Huffman, J. C.; Jackson, S. A.; Eisenstein, O.; Caulton, K. G. *Inorg. Chem.* **1995**, *34*, 488. (c) Caulton, K. G. *New J. Chem.* **1994**, *18*, 25.

(40) Bryndza, H. E.; Tam, W. *Chem. Rev.* **1988**, *88*, 1163.

(41) Langford, C. H.; Gray, H. B. *Ligand Substitution Processes*; W. A. Benjamin, Inc.: Reading, MA, 1966; Chapter 2.

(42) (a) Uehara, Y.; Saito, N.; Yonezawa, T. *Chem. Lett.* **1973**, 495. (b) Orpen, A. G.; Connelly, N. G. *J. Chem. Soc., Chem. Commun.* **1985**, 1310.

(43) Rieger, A. L.; Carpenter, G. B.; Rieger, P. H. *Organometallics* **1993**, *12*, 842.

(44) (a) Messmer, G. G.; Amma, E. L. *Inorg. Chem.* **1966**, *5*, 1775. (b) Rajaram, J.; Pearson, R. G.; Ibers, J. A. *J. Am. Chem. Soc.* **1974**, *96*, 2103. (c) Huffman, J. C.; Laurent, M. P.; Kochi, J. K. *Inorg Chem.* **1977**, *16*, 2639. (d) Carr, S. W.; Shaw, B. L.; Thornton-Pett, M *J. Chem. Soc., Dalton Trans.* **1985**, 2131. (e) Yamashita, H.; Hayashi, T.; Kobayashi, T.; Tanaka, M.; Goto, M. *J. Am. Chem. Soc.* **1988**, *110*, 4417.

oxidatively add to transition metal centers,[6,45] oxidative addition is actually not a typical decomposition pathway taken by halocarbon compounds. A rare example is the complex [Cp*Re(NO)(PPh_3)(CH_2Cl_2)]BF_4 which decomposed at −35 °C to [Cp*Re(NO)(PPh_3)(Cl)(CH_2Cl)]BF_4 in methylene chloride.[28] Presumably, the reason for the general lack of observed oxidative addition reactions lies in the fact that almost all known alkyl and aryl halide complexes are cationic.[46] The barrier to oxidative addition is high enough such that other decomposition pathways are more energetically favorable.

In light of these facts, we studied the decomposition of the PhI complex **4** in diethyl ether and dichloromethane. As mentioned in the Results, **4** decomposed in CD_2Cl_2 slowly at elevated temperatures to a number of products, none of which were the oxidative addition product [($PiPr_3$)$_2$Pt(H)(Ph)(I)]BAr_f or benzene. Similarly, [($PiPr_3$)$_2$Pt(H)(CD_2Cl)(Cl)]BAr_f was not an observed in the decomposition of **3** in CD_2Cl_2. Clean decompositions of **4** as well as its MeI analogue to {*trans*-[($PiPr_3$)$_2$Pt(H)]$_2$(μ-I)}BAr_f (**6**) were observed in *Et_2O*, however, but **6** was not one of the products to which **4** or the MeI adduct decomposed in *CD_2Cl_2*. The mechanism of the reaction shown in eq 7 is obviously enigmatic and has not been addressed here.

The structure of **6** was confirmed in a single crystal X-ray crystallographic study (Figure 4). Although one way to think of **6** might be as an adduct of *trans*-[($PiPr_3$)$_2$Pt(H)]BAr_f with *trans*-($PiPr_3$)$_2$Pt(H)(I), not surprisingly the system is delocalized as evidenced by essentially equivalent Pt−I bond lengths (2.729(3) and 2.737(3) Å).[47] These are longer than the Pt−I bond distance in **4** (2.696(1) Å), but they are in the range usually found for platinum compounds with bridging iodides.[48] Because of the ligand environments, **6** represents the first structurally characterized example of an otherwise unsupported bridging Pt−I−Pt moeity that does not exist as part of an infinite chain structure.

Summary and Conclusions. Protonation of ($PiPr_3$)$_2$Pt(SO_2) with $HBAr_f$ in ether resulted in the labilization of the SO_2 and led to the isolation of the solvent complex, *trans*-[($PiPr_3$)$_2$Pt(H)(OEt_2)]BAr_f (**2**). The latter was used as a precursor in the synthesis of often very labile monodentate halocarbon complexes of the type *trans*-[($PiPr_3$)$_2$Pt(H)(η^1-XR)]BAr_f, a key feature of which is the use of the noncoordinating BAr_f^- counterion. The ability of the platinum center to bind a variety of very weak base donors, including H_2, to form air-stable complexes is a rare feature in coordination complexes, especially those containing alkylphosphines. Such a metal fragment thus might be potentially valuable for molecular detection or separations chemistry. NMR spectroscopy is a simple diagnostic tool here, especially the Pt−H coupling constant, which has been shown to be very sensitive to the nature of the *trans*-ligand.

Crystallographic studies revealed that dichloromethane binds to the cationic Pt center in a monodentate fashion. The structurally characterized *trans*-[($PiPr_3$)$_2$Pt(H)(η^1-BrPh)]BAr_f represents the first example of an isolable transition metal complex containing a monodentate organic bromide ligand. An X-ray crystallographic study performed on *trans*-[($PiPr_3$)$_2$Pt(H)(η^1-IPh)]BAr_f (**4**) revealed an unexpected steric interaction which was suggested by molecular mechanics calculations to be significant. These observations were rationalized in terms of halide-to-metal π bonding in the iodobenzene compound. Interestingly, **4** decomposed on prolonged heating at 100 °C in Et_2O not to the oxidative addition product but rather to the iodide-bridged species {*trans*-[($PiPr_3$)$_2$Pt(H)]$_2$(μ-I)}BAr_f.

The formation of an unstable dihydrogen sigma complex with the cationic Pt(II) center is relevant to recent mechanistic studies by Bercaw and Labinger[49] on C−H activation at very similar centers, e.g., [(tmeda)Pt(CH_3)(OEt_2)]BAr_f (tmeda = *N,N,N′,N′*-tetramethylethylenediamine). These studies relate to oxidation of alkanes by aqueous solutions containing $[PtCl_4]^{2-}$ and $[PtCl_6]^{2-}$ originally studied by Shilov and coworkers and bring into question the existence of σ complexes such as Pt^{II}(RH) as intermediates. Our studies and the initial work by Caulton[23] on $Pt^{II}(H_2)$ complexes indicate by analogy that Pt−alkane complexes surely can exist (at least as transients), and would be expected to be particularly stabilized toward oxidative addition to Pt^{IV}(R)(H) on cationic Pt centers.

Experimental Section

Unless otherwise noted, all reactions and manipulations were performed in dry glassware under a helium atmosphere in a Vacuum Atmospheres drybox or using Schlenk techniques. "Glass bomb" refers to a cylindrical, medium-walled Pyrex vessel joined to a Kontes K-826510 high-vacuum teflon stopcock. All NMR spectra were recorded on a commercial 500 MHz Bruker AMX series spectrometer or a Bruker WM 300 MHz spectrometer. IR spectra were obtained on a Biorad FTS-40 instrument. Elemental analyses were obtained from Oneida Research Services, Inc. Toluene, hexane, Et_2O, and THF were distilled from sodium/benzophenone. Dichloromethane was distilled from calcium hydride. The Pt($PiPr_3$)$_3$,[50] $HBAr_f$ (BAr_f = B(3,5-(CF_3)$_2$$C_6H_3$)$_4$),[51] and *trans*-($PR_3$)$_2$Pt(H)(Cl) (R = *i*-Pr, *t*-Bu)[52] were prepared according to the literature. Iodo- and bromobenzene were dried over activated 4 Å molecular sieves. All other reagents were obtained from commercial suppliers and used without further purification. As a general rule, the drybox catalyst was turned off prior to any reaction in which dichloromethane was used inside the box; use was then followed by purging of the drybox atmosphere.

($PiPr_3$)$_2$Pt(SO_2) (1). Inside the drybox Pt($PiPr_3$)$_3$ (960 mg, 1.42 mmol) was added to a 100 mL Schlenk flask followed by 30 mL of Et_2O. The flask was fitted with a septum and flushed with argon on a schlenk line. A slow flow of SO_2 was added through a needle over the top of the orange solution which immediately turned deep green. The flow was continued for 10 min after which the SO_2-saturated solution was allowed to stand at room temperature for an additional 45 min. The volatiles were then removed under vacuum leaving a green powder. Inside the drybox this powder was extracted with 30 mL of warm hexane. The deep green solution was filtered and then reduced to 20 mL under vacuum. Green crystalline product (771 mg, 94% yield) was isolated after allowing the solution to stand in a freezer (−30 °C) overnight. This reaction was performed using as little as 3 equiv of SO_2, added by vacuum transfer, without a decrease in yield:

(45) Collman, J. P.; Hegedus, L. S.; Norton, J. R.; Finke, R. G. *Principles and Applications of Organotransition Metal Chemistry*; University Science Books: Mill Valley, CA, 1987; pp 306−322.

(46) For examples of neutral chelating halocarbon compounds, see: (a) Reference 7. (b) Lahuerta, P.; Latorre, J.; Martinez-Manez, R.; Sanz, F. *J. Organomet. Chem.* **1988**, *356*, 355. (c) Solans, X.; Font-Albana, M.; Aguilo, M.; Miravitlles, C.; Besteiro, J. C.; Lahuerta, P. *Acta Crystallogr., C* **1985**, *41*, 841.

(47) If **6** were an adduct of these discrete molecules, the significantly different Pt−I bond distances would be expected as is most often observed in infinite chains of repeating mixed valent bridging iodide complexes due to the Peierls effect. The type of disorder in the position of the bridging iodide that would be expected for random crystallization of a Pt−I···Pt species was not observed. See, for example: (a) Weinrach, J. B.; Ekberg, S. A.; Conradson, S. D.; Swanson, B. I. *Inorg. Chem.* **1990**, *29*, 981. (b) Matsumoto, N.; Yamashita, M.; Kida, S. *Acta Crystallogr.* **1979**, *B35*, 1458.

(48) (a) Toronto, D. V.; Balch, A. L. *Inorg. Chem.* **1994**, *33*, 6132. (b) Casas, J. M.; Falvello, L. R.; Forniés, J.; Martín, A.; Tomás, M. *J. Chem. Soc., Dalton Trans.* **1993**, 1107. (c) Bennett, M. A.; Berry, D. E.; Bhargava, S. K.; Ditzel, E. J.; Robertson, G. B; Willis, A. C. *J. Chem. Soc., Chem. Commun.* **1987**, 1613. (d) Ling, S. S. M.; Jobe, I. R.; Galas, A. M. R.; Hursthouse, M. B. *J. Chem. Soc., Dalton Trans.* **1983**, 1583.

(49) (a) Holtcamp, M. W.; Labinger, J. A.; Bercaw, J. E., submitted. (b) Stahl, S. S.; Labinger, J. A.; Bercaw, J. E. *J. Am. Chem. Soc.* **1995**, *118*, 5961.

(50) Yoshida, T.; Matsuda, T.; Otsuka, S. *Inorg. Synth.* **1979**, *19*, 108.

(51) Brookhart, M.; Grant, B.; Volpe, A. F., Jr. *Organometallics* **1992**, *11*, 3920.

(52) Goel, A. B.; Goel, S. *Inorg. Chim. Acta* **1982**, *65*, L77.

^{1}H NMR (C_6D_6) δ 2.20 (m, 6H, CH), 1.19 (vq = virtual quartet, J_{HP} = 7.2, 36H, CH_3); $^{13}C\{^1H\}$ NMR (CD_2Cl_2) δ 26.33 (vt, J_{CP} = 12.7, CH), 20.77 (s, CH_3); $^{31}P\{^1H\}$ NMR (C_6D_6) δ 61.83 (s, J_{PPt} = 4189.4); IR (KBr, cm^{-1}) ν(SO) = 1176, 1035. Anal. Calcd for $C_{18}H_{42}O_2P_2PtS$: C, 37.30; H, 7.30. Found: C, 37.38; H, 7.25.

[(PiPr$_3$)$_2$Pt(H)(OEt$_2$)]BAr$_f$ (2). ($PiPr_3)_2Pt(SO_2$) (254 mg, 0.438 mmol) was added to a 100 mL Schlenk flask followed by 20 mL of Et_2O in the drybox. A separate 25 mL Schlenk flask was charged with 469 mg of $HBAr_f$ (0.463 mmol) and 15 mL of Et_2O. Hexane (25 mL) was added to a third flask. The three flasks were fitted with septa and flushed with argon on a Schlenk line. The green solution containing the platinum complex was cooled to −78 °C in a dry ice/acetone bath after which the $HBAr_f$ solution was added slowly by cannula under argon. The solution immediately turned yellow and was stirred at −78 °C for 15 min. The hexane was then added under argon by syringe. The resulting solvent mixture was reduced to 25 mL under vacuum during which time yellow powder precipitated. After allowing the mixture to stand at −78 °C for 30 min, the pale yellow solution was decanted by syringe. The remaining yellow powder was dried under vacuum (595 mg, 93% yield): ^{1}H NMR (CD_2Cl_2, −83 °C) δ 7.72 (s, 8H, BAr_f), 7.53 (s, 4H, BAr_f), 3.74 (q, J = 6.8, 4H, ether CH_2), 2.24 (br, 6H, CH), 1.30 (t, J_{HH} = 6.8, 6H, ether CH_3), 1.13 (vq, J = 6.4, 36H, iPr CH_3), −27.84 (t, J_{HP} = 14, J_{HPt} = 1540, 1H, PtH); $^{13}C\{^1H\}$ NMR (CD_2Cl_2, −83 °C) δ 161.42 (q, J = 49.0, *i*-BAr_f), 134.18 (s, *o*-BAr_f), 128.18 (qm, J_{CF} = 31.1, *m*-BAr_f), 124.0 (d, J_{CF} = 272.8, CF_3), 117.13 (s, *p*-BAr_f), 70.37 (s, CH_2), 25.38 (vt, J_{CP} = 15.3, CH), 19.23 (s, *i*-Pr CH_3), 14.76 (s, ether CH_3); $^{31}P\{^1H\}$ NMR (CD_2Cl_2, −58 °C) δ 55.48 (s, J_{PPt} = 2748). Satisfactory elemental analysis could not be obtained.[18]

[(PiPr$_3$)$_2$Pt(H)(η^1-ClCH$_2$Cl)]BAr$_f$ (3). Method A. Complex **3** was isolated by recrystallizing the Et_2O complex **2** from CH_2Cl_2/hexane. For example, **3** was isolated as yellow plates (517 mg, 80% yield) when a CH_2Cl_2 solution of **2** (642 mg in 4 mL) was layered with 8 mL of hexane and allowed to stand at −30 °C overnight. The deuterium analog was prepared by substituting CD_2Cl_2 for CH_2Cl_2. The static complex **3** was not observed by NMR spectroscopy (see Results). The following data represent the solvent exchange averaged resonances when **3** was dissolved in CD_2Cl_2: ^{1}H NMR (CD_2Cl_2, −58 °C) δ 2.34 (m, 6H, CH), 1.19 (m, 36H, CH_3), −22.82 (t, J_{HP} = 11.9, J_{HPt} = 1852, 1H, PtH); $^{13}C\{^1H\}$ NMR (CD_2Cl_2, −78 °C) δ 24.51 (m, CH), 19.17 (s, CH_3), the ^{1}H and ^{13}C resonances attributed to the counterion were identical to those reported for **2**; $^{31}P\{^1H\}$ NMR (CD_2Cl_2, −58 °C) δ 54.61 (s, J_{PPt} = 2637); IR (mineral oil, cm^{-1}) $\nu(CCl)_{asym}$ = 751, $\nu(CCl)_{sym}$ = 663. Satisfactory elemental analysis could not be obtained due to the instability of the compound toward CH_2Cl_2 loss.

Method B. In the drybox *trans*-$(PiPr_3)_2Pt(H)(Cl)$ (754 mg, 1.37 mmol) was dissolved in 25 mL of CH_2Cl_2 (see note in general section of the Experimental Section) in a round bottom flask. $NaBAr_f$[51] (1.26 g, 1.42 mmol) was then added as a solid with stirring. The homogeneous yellow solution quickly turned cloudy orange and was allowed to stir at room temperature for 2 h. The mixture was filtered through Celite to remove the NaCl, reduced in volume under vacuum to 4 mL, layered with 6 mL of hexane, and placed in a −30 °C freezer. Yellow crystalline **3** was isolated in 63% yield.

[(PiPr$_3$)$_2$Pt(H)(η^1-IPh)]BAr$_f$ (4). This reaction was performed in the drybox. The Et_2O complex **2** (123 mg, 8.05×10^{-5} mol) was added to a 50 mL round bottom flask with a stir bar and dissolved in 15 mL of dichloromethane. A solution of iodobenzene (103 mg, 0.505 mmol, 6.3 equiv) was added slowly with stirring. After standing at room temperature for 3 h the volume was reduced to 5 mL. This yellow solution was layered with 5 mL of hexane and placed in a −30 °C freezer. Over 12 h time, colorless crystals precipitated (122 mg, 87% yield) which were dried under vacuum: ^{1}H NMR (CD_2Cl_2) δ 7.72 (s, 8H, BAr_f), 7.56 (s, 4H, BAr_f), 7.66 (d, J = 8.1, 2H, Ph), 7.51 (t, J = 7.2, 1H, Ph), 7.26 (vt, J = 7.6, 2H, Ph), 2.30 (m, 6H, CH), 1.24 (vq, J = 7.2, 36H, CH_3), −17.02 (vbr, J_{HPt} = 1650, 1H, PtH) (at −93 °C, the hydride appeared as a triplet at −15.89 (J_{HP} = 9, J_{HPt} = 1654)); $^{13}C\{^1H\}$ NMR (CD_2Cl_2) δ 161.99 (q, J = 49.8, *i*-BAr_f), 137.21 (s, Ph), 135.08 (s, *o*-BAr_f), 131.61 (s, Ph), 130.77 (s, Ph), 129.20 (q, J_{CF} = 31.5, *m*-BAr_f), 124.90 (d, J_{CF} = 271.7, CF_3), 117.76 (s, *p*-BAr_f), 27.05 (vt, J_{CP} = 15.0, CH_2), 20.38 (s, CH_3); $^{31}P\{^1H\}$ NMR (CD_2Cl_2) δ 53.03 (s, J_{PPt} = 2603.8); IR (mineral oil, cm^{-1}): peaks for bound PhI were found at 1569, 1011, 994, and 652. All other iodobenzene bands were obscured by those assigned to the BAr_f counterion. Anal. Calcd for $C_{56}H_{60}BF_{24}IP_2Pt$: C, 42.47; H, 3.82. Found: C, 42.74; H, 3.70.

[(PiPr$_3$)$_2$Pt(H)(η^1-BrPh)]BAr$_f$ (5). Inside the drybox the Et_2O complex **2** (69.0 mg, 5.00×10^{-5} mol) was dissolved in 0.8 mL of CH_2Cl_2. Bromobenzene (125 μL, 1.187 mmol, 24 equiv) was then added by syringe. The yellow solution was layered with 1 mL of hexane and placed in a −30 °C freezer. Very pale yellow crystals were isolated after 1 day (46 mg, 60% yield). The static complex **5** was not observed by NMR spectroscopy (see Results). The following data represent the solvent exchange averaged resonances when seven equivalents of PhBr were added to **3** in CD_2Cl_2: ^{1}H NMR (CD_2Cl_2, −58 °C) δ 7.48 (d, J = 8.0, 2H, Ph), 7.32 (m, 1H, Ph), 7.25 (vt, J = 7.6, 2H, Ph), 2.24 (m, 6H, CH), 1.19 (vq, J = 7.2, 36H, CH_3), −20.74 (br, J_{HPt} = 1781, 1H, PtH); $^{13}C\{^1H\}$ NMR (CD_2Cl_2, −10 °C) δ 131.78 (s, Ph), 130.61 (s, Ph), 130.58 (s, Ph), 26.01 (br, CH), 20.04 (br m, CH_3); the signals for BAr_f were identical to those for **2**; $^{31}P\{^1H\}$ NMR (CD_2Cl_2, −58 °C) δ 52.28 (s, J_{PPt} = 2627); IR (mineral oil, cm^{-1}): peaks for bound PhBr were found at 1571, 1017, 998, and 457. All other bromobenzene peaks were obscured by those assigned to the BAr_f counterion. The instability of **5** prevented a satisfactory elemental analysis.

{***trans*-[(PiPr$_3$)$_2$Pt(H)]$_2$(μ-I)}BAr$_f$ (6).** A 25 mL bomb was charged with **4** (193 mg, 1.22×10^{-4} mol) followed by 10 mL of Et_2O in the drybox. The closed flask was then removed from the drybox and placed in an oil bath at 100 °C for four days, during which time the pale yellow solution turned orange. The volatile materials were removed under vacuum to afford a sticky orange-red solid which was washed with hexane (2 × 8 mL) and subsequently isolated as a dark orange powder. The powder was dissolved in 1.5 mL of CH_2Cl_2, layered with 1.5 mL of hexane, and placed in a −30 °C freezer. Thin yellow hexagonal plates were isolated (colorless after a second recrystallization). The mother liquor was pumped to dryness and a second crop isolated by recrystallization from Et_2O hexane in the same manner. The total yield was 96 mg (39%): ^{1}H NMR (CD_2Cl_2) δ 2.47 (m, 12H, CH), 1.27 (vq, J = 7.2, 72H, CH_3), −18.40 (br, J_{HPt} = 1645, 2H, PtH); $^{13}C\{^1H\}$ NMR (CD_2Cl_2) δ 27.14 (vt, J_{CP} = 15.3, CH), 20.59 (s, CH_3); the signals for BAr_f were identical to those for **4**; $^{31}P\{^1H\}$ NMR (CD_2Cl_2) δ 53.06 (s, J_{PPt} = 2738); FAB MS (NOBA) *m/e* (relative intensity) 1159 ([M − BAr_f]$^+$, 40), 516 ([M − $(PiPr_3)_2Pt(H)(I)$ − BAr_f]$^+$, 100).

[(PiPr$_3$)$_2$Pt(H)(THF)]BAr$_f$ (7). Complex **2** (40 mg, 2.75×10^{-5} mol) was dissolved in 0.8 mL of THF in the drybox. The solution was then layered with 1 mL of hexane. After allowing the solution to stand overnight in a −30 °C freezer, colorless crystals of **7** were isolated which were dried under vacuum (31 mg, 78% yield): ^{1}H NMR (CD_2Cl_2) δ 3.84 (m, 4H, CH_2), 2.32 (m, 6H, CH), 1.94 (m, 4H, CH_2), 1.29 (vq, J = 7.2, 36H, CH_3), −27.88 (−10 °C, br, J_{HPt} = 1524, 1H, PtH); $^{13}C\{^1H\}$ NMR (CD_2Cl_2, −10 °C) δ 74.38 (br s, THF), 26.12 (vt, J_{CP} = 14.6, CH), 25.60 (s, THF), 20.10 (s, CH_3); the signals for BAr_f were identical to those for **4**; $^{31}P\{^1H\}$ NMR (CD_2Cl_2) δ 57.10 (s, J_{PPt} = 2755). Anal. Calcd for $C_{54}H_{63}BF_{24}OP_2Pt$: C, 44.67; H, 4.37. Found: C, 44.89; H, 4.39.

[(P-*t*-Bu$_3$)$_2$Pt(H)]BAr$_f$. In the drybox, *trans*-(P-*t*-$Bu_3)_2Pt(H)(Cl)$ (639 mg, 1.00 mmol) was added to a round bottom flask with a stir bar. Diethyl ether (20 mL) was added to form a pale yellow suspension. To this was added $NaBAr_f$[57] (901 mg, 1.02 mmol) piecewise as a solid with stirring during which time the mixture turned yellow-orange. After stirring at room temperature for two hours, the volatile materials were removed under vacuum and the resulting yellow powder was extracted with 25 mL of CH_2Cl_2. The dark orange mixture was filtered through Celite to remove the NaCl and concentrated under vacuum to 16 mL. This solution was layered with 16 mL of hexane and placed in a −30 °C freezer. Pure [(P-*t*-$Bu_3)_2Pt(H)]BAr_f$ was isolated as a yellow powder in 64% yield (941 mg): ^{1}H NMR (CD_2Cl_2) δ 1.51 (vt, J = 6.4, 54H, *t*-Bu), −36.53 (t, J_{HP} = 8.0, J_{HPt} = 2605, 1H, PtH); $^{13}C\{^1H\}$ NMR (CD_2Cl_2) δ 41.07 (t, J_{CP} = 8.9, $C(CH_3)_3$), 32.75 (s, $C(CH_3)_3$); the signals for BAr_f were identical to those for **4**; $^{31}P\{^1H\}$ NMR (CD_2Cl_2) δ 87.14 (s, J_{PPt} = 2625). Anal. Calcd for $C_{56}H_{67}BF_{24}P_2Pt$: C, 45.95; H, 4.61. Found: C, 46.11; H, 4.55.

Reaction of 3 with H$_2$. Complex **3** (15 mg, 1.02×10^{-5} mol) was loaded into an NMR tube followed by 0.5 mL of CD_2Cl_2 in the drybox.

The tube was then attached to a Kontes vacuum adaptor via a Cajon joint. A calculated quantity of dihydrogen was added by transferring a measured pressure (ideal gas law) of gas into the NMR tube at 77 K utilizing a MKS baratron gauge attached to a high-vacuum line (485 Torr at 77 K, 2.83×10^{-4} mol, 28 equiv). The tube was then flame sealed using an oxygen/propane torch, and immediately transferred to a dewar packed with dry ice for transport to the NMR spectrometer, with the probe precooled to −80 °C. An identical reaction was set up in which H_2 was replaced with HD in order to determine the ligated HD coupling constant (33.7 Hz). The NMR resonances are described in the Results.

X-ray crystal structure determinations. A crystal of **3**, **4**, **5**, **6**, or **7** was mounted on a thin glass fiber using silicone grease. The crystal, which was mounted from a pool of mineral oil bathed in argon, was then immediately placed under a liquid N_2 stream on a Siemens P4/PC diffractometer. The radiation used was graphite monochromatized MoKα radiation ($\lambda = 0.710\,69$ Å). The lattice parameters were optimized from a least-squares calculation on 25 (32 for **3**, **6**, and **7**) carefully centered reflections of high Bragg angle. The data was collected using ω scans over a 0.80−1.18° scan range. Three check reflections monitored every 97 reflections showed no systematic variation of intensities. For **6**, data were collected only to $2\theta = 40°$ due to the small size of the crystal. Lattice determination and data collection were carried out using XSCANS Version 2.10b software. All data reduction, including Lorentz and polarization corrections and structure solution and graphics were performed using SHELXTL PC Version 4.2/360 software. The structure refinement was performed using SHELX-93 software.[53] The data were corrected for absorption using the ellipsoid option in the XEMP facility of SHELXTL PC.

The space groups were uniquely determined from the systematic absenses. In the case of **3**, **6**, and **7** the Pt, Pt−bound heteroatom, and P atoms as well as the majority of C atoms were located from the direct methods solution. The remaining C atoms and the B and F atoms were located during subsequent Fourier synthesis. For **3**, it was at this time that significant electron density was observed near some F atoms; these residual peaks were modeled as disordered F at one-half occupancy and labled as primed F atoms. A disordered region near the Pt atom was then modeled as two disordered methylene chloride molecules. These two molecules, labeled Cl(2)−C(45)−Cl(1) and Cl(3)−C(45′)−Cl(1), were refined with their site occupancy factors tied to one. In the final refinement the occupancy factors refined to 0.677(8) for the Cl(2)−C(45)−Cl(1) molecule and 0.323(8) for the Cl(3)−C(45′)−Cl(1) molecule. It was discovered at this time that the disorder in the methylene chloride was accompanied by disorder in the closest isopropyl group [C(8)−C(3)−C(9)]. This disorder was modeled as two half occupancy isopropyl groups, C(8)−C(3)−C(9) and C(8′)−C(3′)−C(9′). For **3**, **6**, and **7** the next step was a high angle refinement to locate the Pt−hydrides. The weighting function w was multipled by $1 - \exp[-5(\sin\theta/\lambda)^2]$ in order to weight the high angle data prior to analysis of the difference map. This tactic revealed all hydrogen atoms in the structure. The positional coordinates of the hydride peak, approximately 1.7 Å (**3**), 1.4 Å (**6**), or 1.5 Å (**7**) from the Pt and in a square plane with the two P atoms and the Pt−bound heteroatom, were refined with the temperature factor fixed at 0.08 Å^2. All remaining hydrogen atoms were fixed in positions of ideal geometry, with a C−H distance of 0.96 Å for CH_3 hydrogens, 0.97 Å for the CH_2 hydrogens, and 0.98 Å for the CH hydrogens and refined using the riding model in the HFIX facility in SHELXL 93. These idealized hydrogen atoms had their isotropic temperature factors fixed at 1.2 times (CH) or 1.5 times (CH_3) the equivalent isotropic U of the C atoms to which they were bonded.

For the aryl halide complexes **4** and **5**, Patterson techniques were used to locate the platinum, halide, and phosphorous atoms. All remaining atoms were found from subsequent difference maps. The phenyl group was refined as a rigid body, with ring carbon−carbon distances fixed at 1.39 Å. All hydrogen atoms were fixed in positions of ideal geometry. The C−H distances were fixed at 0.980 Å (tertiary), 0.970 Å (phenyl), or 0.960 Å (methyl). All hydrogen atoms were refined using the riding model in the HFIX facility in SHELX-93, and had their isotropic temperature factors fixed at 1.2 (tertiary and phenyl) or 1.5 (methyl) times the equivalent isotropic *U* of the atom they were bonded to. The final refinement[54] for all compounds included anisotropic thermal parameters on all non-hydrogen atoms.

Molecular Mechanics. The molecular structure of *trans*-[$(PiPr_3)_2$-Pt(H)(η^1-IPh)]$^+$ was minimized using the ESFF force field within Discover 95.0.[37] The optimization routine within the Builder module was used with the charges option turned on. Since ESFF does not have force field parameters for a hydride ligand, a fluoride ion was used in its place with the default distance of 1.623 Å. Force field parameters for Pt(II) in a square planar geometry were used (Pt024 switch). Charges on the platinum and fluoride ions were set at +2 and −1, respectively. All other atoms were left with neutral charges. The initial starting point for the minimization was the crystal coordinates of the [$(PiPr_3)_2$Pt(H)(η^1-IPh)]$^+$ ion with the hydride replaced with a fluoride ion (*vide supra*). Convergence was achieved (maximum derivative 0.00605) after 34 iterations of steepest descent and 309 iterations of quasi Newton (BFGS). The initial and final energies were 61.869 and 51.419 kcal, respectively. Starting and ending structures are summarized in Figure 7 and Table 5. A second minimization was performed using the final structure of the first minimization with the dihedral angle C(6)−C(1)−I(1)−Pt(1) = 0°. This minimization led to a structure with a final energy 1.5 kcal below the structure found in the first minimization, but was chemically unreasonable due to a Pt coordination geometry with trans angles of 149.6° and 146.2°.

Acknowledgment. This work was supported by the Office of Basic Energy Sciences of the DOE and the Los Alamos National Laboratory Directed Research and Development Office.

Supporting Information Available: Complete details of the structural determinations of compounds **3**, **4**, **5**, **6**, and **7** and an ORTEP drawing of the BAr_f anion in **3** (53 pages). See any current masthead page for ordering and Internet access instructions.

JA961836Y

(53) XSCANS and SHELXTL PC are products of Siemens Analytical X-ray Instruments, Inc., 6300 Enterprise Lane, Madison, WI 53719. SHELX-93 is a program for crystal structure refinement written by G. M. Sheldrick University of Göttingen, Germany, 1993.

(54) $R1 = \sigma||F_o| - |F_c||/\sigma|F_o|$ and $R2_w = [\Sigma[w(F_o^2 - F_c^2)^2]/\Sigma[w(F_o^2)^2]]^{1/2}$. The parameter $w = 1/[\sigma^2(F_o^2) + (0.0397P)^2 + 14.2032P]$ for **3**, $1/[\sigma^2(F_o^2) + (0.0857P)^2 + 5.2066P]$ for **4**, $1/[\sigma^2(F_o^2) + (0.0639P)^2 + 34.2822P]$ for **5**, $1/[\sigma^2(F_o^2) + (0.0482P)^2 + 97.7170P]$ for **6**, and $1/[\sigma^2(F_o^2) + (0.0273P)^2 + 18.3466P]$ for **7**, where $P = (F_o^2 + 2F_c^2)/3$.